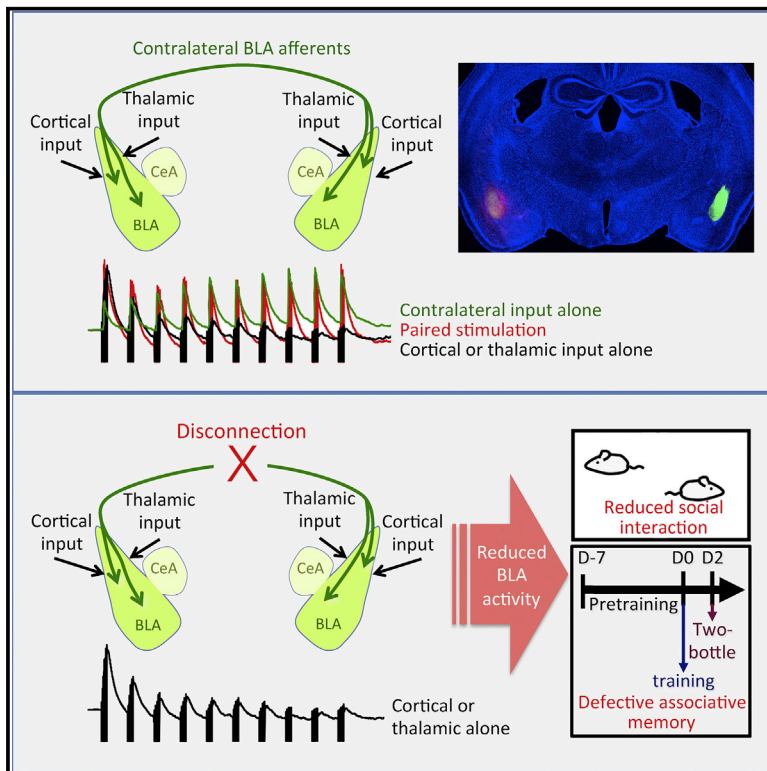


Interhemispheric Connectivity Potentiates the Basolateral Amygdalae and Regulates Social Interaction and Memory

Graphical Abstract



Authors

Tzyy-Nan Huang, Tsan-Ting Hsu, Ming-Hui Lin, ..., Mi-Hua Tao, John Y. Lin, Yi-Ping Hsueh

Correspondence

yph@gate.sinica.edu.tw

In Brief

Huang et al. show that contralateral innervation between two basolateral amygdalae (BLA) in the two brain hemispheres evokes the synaptic activity of BLA and intensifies the BLA response to ipsilateral afferents, including cortical and thalamic inputs. BLA contralateral connectivity is required for amygdala-dependent behaviors, including social interaction and memory.

Highlights

- Basolateral amygdalae (BLA) project to both contralateral BLA and ipsilateral CeA
- Contralateral BLA form monosynaptic innervations and mutually activate one another
- Contralateral BLA input facilitates synaptic responses of BLA to ipsilateral inputs
- Disruption of BLA contralateral connectivity impairs social behaviors and memory



Interhemispheric Connectivity Potentiates the Basolateral Amygdalae and Regulates Social Interaction and Memory

Tzzy-Nan Huang,^{1,4} Tsan-Ting Hsu,^{1,4} Ming-Hui Lin,¹ Hsiu-Chun Chuang,^{1,5} Hsiao-Tang Hu,¹ Cheng-Pu Sun,² Mi-Hua Tao,² John Y. Lin,³ and Yi-Ping Hsueh^{1,6,*}

¹Institute of Molecular Biology, Academia Sinica, Taipei 11529, Taiwan, ROC

²Institute of Biomedical Sciences, Academia Sinica, Taipei 11529, Taiwan, ROC

³School of Medicine, University of Tasmania, TAS 7000, Australia

⁴These authors contributed equally

⁵Present address: Department of Molecular and Cell Biology, University of California, Berkeley, Berkeley, CA 94720, USA

⁶Lead Contact

*Correspondence: yph@gate.sinica.edu.tw

<https://doi.org/10.1016/j.celrep.2019.08.082>

SUMMARY

Impaired interhemispheric connectivity is commonly found in various psychiatric disorders, although how interhemispheric connectivity regulates brain function remains elusive. Here, we use the mouse amygdala, a brain region that is critical for social interaction and fear memory, as a model to demonstrate that contralateral connectivity intensifies the synaptic response of basolateral amygdalae (BLA) and regulates amygdala-dependent behaviors. Retrograde tracing and c-FOS expression indicate that contralateral afferents widely innervate BLA non-randomly and that some BLA neurons innervate both contralateral BLA and the ipsilateral central amygdala (CeA). Our optogenetic and electrophysiological studies further suggest that contralateral BLA input results in the synaptic facilitation of BLA neurons, thereby intensifying the responses to cortical and thalamic stimulations. Finally, pharmacological inhibition and chemogenetic disconnection demonstrate that BLA contralateral facilitation is required for social interaction and memory. Our study suggests that interhemispheric connectivity potentiates the synaptic dynamics of BLA neurons and is critical for the full activation and functionality of amygdalae.

INTRODUCTION

The connectivity between two brain hemispheres is critical for brain functions, such as the integration of sensory input, cognition, and emotion processing (Aboitiz and Montiel, 2003; Fenlon and Richards, 2015). Abnormal long-range connectivity is often associated with neurodevelopmental or neuropsychiatric disorders, such as autism spectrum disorders (ASDs) (Frazier and Hardan, 2009; Geschwind and Levitt, 2007), schizophrenia

(Arnone et al., 2008; Ribolsi et al., 2014), attention-deficit/hyperactivity disorder (Valera et al., 2007), dyslexia (Dhar et al., 2010), and depression (Xu et al., 2013). Interhemispheric connections are mainly achieved by four major commissures— anterior commissure (AC), corpus callosum, hippocampal commissure, and posterior commissure (Lindwall et al., 2007). These commissures are highly conserved in vertebrates, reinforcing their crucial roles in the function of vertebrate brains (Suárez et al., 2014).

Amygdalae are critical for social interaction, fear memory, and anxious behaviors (Janak and Tye, 2015; LeDoux et al., 2017; Tovote et al., 2015). In mice, the basolateral amygdalae (BLA) form ipsilateral connections with other brain regions, such as the medial prefrontal cortex, auditory cortex, insular cortex, entorhinal cortex, nucleus accumbens, and ventral hippocampus, and deliver the signals to the central amygdalae (CeA) (Ferreira et al., 2005; Janak and Tye, 2015; Miranda and McGaugh, 2004; Osorio-Gomez et al., 2017; Roozendaal et al., 2009). In addition, amygdalae receive intensive axonal projection from contralateral amygdalae and weaker signals from contralateral insular cortex and entorhinal cortex via the posterior part of the AC in mice (Huang et al., 2014; Jouandet and Hartenstein, 1983). However, the physiological significance of these contralateral connectivities remains elusive.

Our previous study showed that *Tbr1*^{+/-} mice, a mouse model of ASD, lack the posterior part of the AC and exhibit autism-like behaviors (Huang et al., 2014, 2019). TBR1, encoded by a causative gene for ASD (De Rubeis et al., 2014; Neale et al., 2012; O’Roak et al., 2012a, 2012b; Sanders et al., 2015), is specifically expressed in projection neurons (PNs) of the BLA, cerebral cortex, hippocampus, and olfactory bulb (Bulfone et al., 1995; Hevner et al., 2001; Huang et al., 2014). Loss of one copy of *Tbr1* alters the expression of *Ntn1*, *Cntn2*, *Cdh8*, and *Grin2b* and disrupts the axonal projection and activation of amygdalar neurons (Chuang et al., 2014, 2015; Huang et al., 2014). Neuronal activation of the BLA upon behavioral stimulation is impaired in *Tbr1*^{+/-} mice (Huang et al., 2014). Enhancing *N*-methyl-D-aspartate receptor (NMDAR) activity using D-cycloserine (a coagonist of NMDAR)



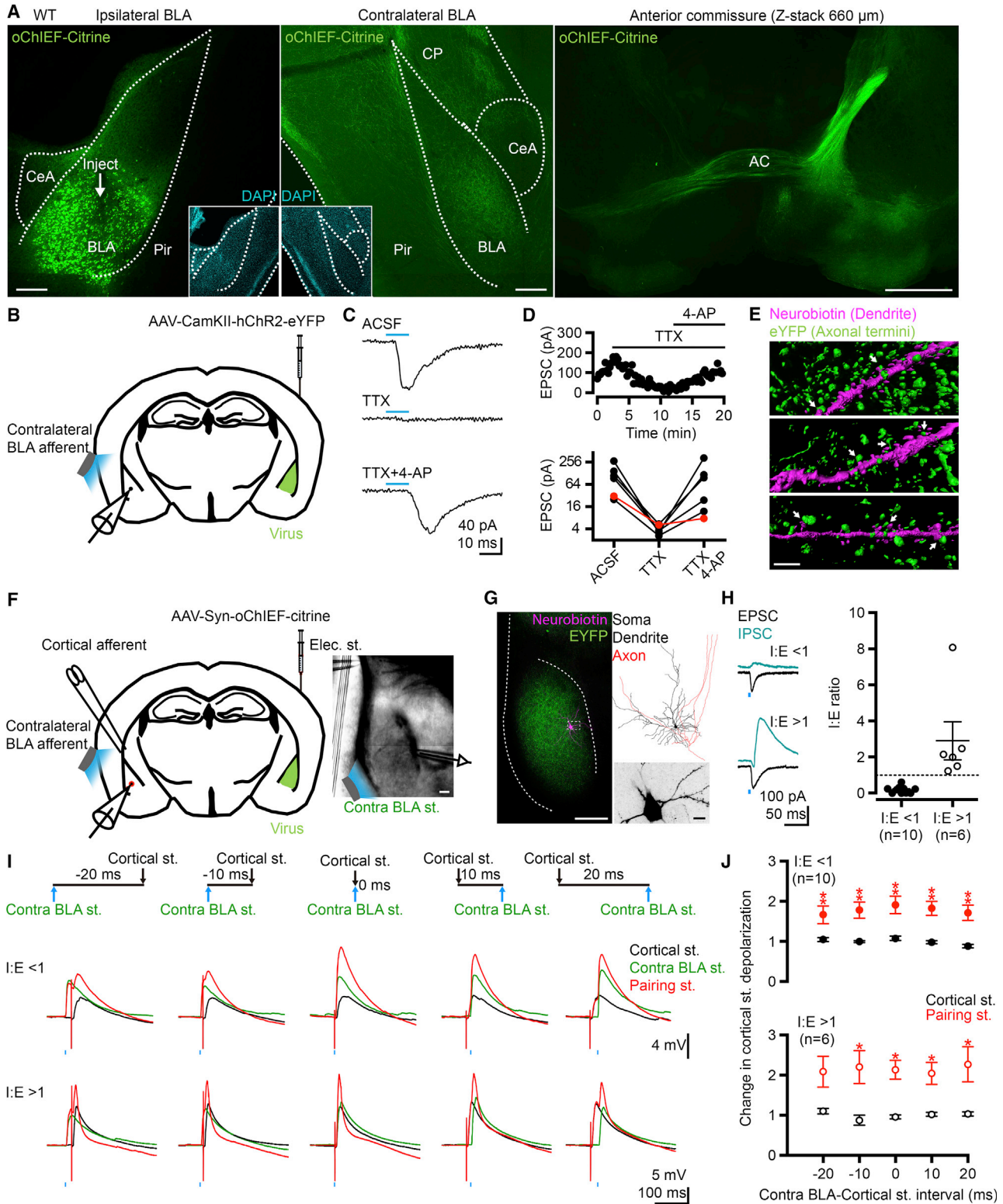


Figure 1. Potentiation of Cortical-BLA Postsynaptic Potentials by Contralateral BLA Inputs

(A) AAV was unilaterally infected to BLA of wild-type mice to outline the axonal projection of BLA. DAPI signals were used to define the brain regions. AC, anterior commissure; BLA, basolateral amygdala; CeA, central amygdala; CP, caudate-putamen; Pir, piriform cortex.

(legend continued on next page)

or clioquinol (a zinc chelator promoting transsynaptic transportation of zinc) ameliorates the autistic behaviors of *Tbr1*^{+/-} mice (Huang et al., 2014, 2019; Lee et al., 2015). Based on these studies, we hypothesized that interhemispheric connectivity delivers a positive signal for the full activation of both BLA in the two brain hemispheres and controls amygdala-regulated functions, such as social interaction and associative memory. In this report, we used mouse models and diverse optogenetic, electrophysiological recording, cell biology, and mouse behavior analyses to investigate this hypothesis.

RESULTS

Monosynaptic Innervation to BLA Neurons by Contralateral Afferents

We first applied optogenetic approaches to investigate the properties of BLA contralateral connectivity. The adeno-associated viral (AAV8) vector that expresses various channelrhodopsins tagged with fluorescent proteins was unilaterally infected into BLA. Expression patterns of channelrhodopsin-fluorescent proteins were first examined based on the signals of fluorescent proteins. When AAV was unilaterally delivered to BLA neurons (Figure 1A, left), axons of these infected cells outlined by channelrhodopsin-fluorescent proteins extended to the ipsilateral side and the contralateral BLA via the posterior part of the AC (Figure 1A, center and right; Video S1). Misinjection of AAV to the CeA or other neighboring regions of BLA did not result in noticeable contralateral projection to the BLA (Figures S1A and S1C; Video S2). Echoing our previous study (Huang et al., 2014), *Tbr1*^{+/-} mice did not reveal contralateral axonal projection of BLA via the AC (Figure S1B; Video S3), further supporting the contralateral projection deficit of BLA in *Tbr1*^{+/-} mice. Using this setup, we investigated the response of BLA to input derived from contralateral BLA.

After unilateral infection with AAV8-CaMKII-hChR2-eYFP (Lee et al., 2010), whole-cell voltage-clamp recording at the contralateral BLA was performed with blue light stimulation (Figure 1B). All six recorded neurons responded to blue light and their responses were blocked by tetrodotoxin (TTX, a voltage-gated Na⁺ channel blocker) (Figures 1C and 1D). In five of the six recorded neurons, the optically evoked monosynaptic excitatory postsynaptic current (EPSC) reoccurred after blocking K⁺ shunting by 4-aminopyridine (4-AP, a broad-spectrum K⁺ channel inhibitor) (Figures 1C and 1D), suggesting that BLA neurons are able to receive monosynaptic transmission from the contralateral hemisphere. Based on neurobiotin labeling, which had been injected into recorded neurons post hoc, contralateral axonal termini (labeled by enhanced yellow fluorescent protein [eYFP]) frequently contacted the dendritic spines of BLA neurons (i.e., the subcellular structures of excitatory synapses) (Figure 1E; Videos S4, S5, and S6). These results suggest that contralateral axonal termini expressing hChR2-eYFP directly contact and deliver excitatory synaptic transmission to BLA PNs.

Potentiation of BLA Responses to Cortical Stimulation by Contralateral Inputs

We further investigated whether the stimulation of contralateral BLA afferents potentiates synaptic responses of BLA PNs. An ultra-fast channelrhodopsin (ChR) variant oChIEF-expressing AAV (Lin et al., 2009) was unilaterally delivered to the BLA for whole-cell current-clamp recordings at the contralateral BLA (Figure 1F). PNs were identified based on their morphological feature of dense spiny dendrites (Figure 1G) and electrophysiological properties (Figure S2) (Sosulina et al., 2006). To account for the contribution of circuit-driven inhibition, we stimulated contralateral BLA with the strongest light intensity (6.6 mW/mm²) in our device to increase the possibility of recruiting maximal interneuron populations (Hsu et al., 2016). After examining the effect

(B) Experimental design of contralateral optical stimulation and whole-cell recordings of postsynaptic neurons 3 weeks after the unilateral infection of AAV into the BLA.

(C) Example traces of a light-evoked EPSC recorded in a contralateral BLA neuron. $V_{\text{hold}} = -70$ mV, near the IPSC reversal potential; $[\text{Cl}^-]_i = 8.75$ mM. Top, artificial cerebrospinal fluid (ACSF); center, TTX (1 μM) application; bottom, addition of 4-AP (1 mM) during TTX application. Traces are averages of 5 sweeps for each condition.

(D) Top, time course for the experiment shown in (C); bottom, summary plots of the effects of TTX and TTX plus 4-AP on light-evoked EPSCs ($n = 6$ from 4 mice). Red circle-line indicates the neuron with no monosynaptic component.

(E) Imapris 3D reconstructions of confocal images after recording in (B). Three dendritic segments labeled with neurobiotin (magenta) are shown. The white arrows indicate the appositions of eYFP⁺ axonal termini to the postsynaptic dendritic spines. The 3D structures are available in Videos S4, S5, and S6.

(F) Schematic (left) and infrared-differential interference contrast (IR-DIC) image (right) showing the experimental design of the electrical stimulation (denoted "st." in the figure) of cortical afferents paired with contralateral BLA optical stimulation while recording from putative projection neurons (defined by electrophysiological properties summarized in Figure S2) 3 weeks after unilateral infection with oChIEF-expressing AAV into the BLA.

(G) An example of a recorded projection neuron labeled post hoc with neurobiotin. Left, the original confocal image. Upper right, reconstructed neuronal image based on the neurobiotin signal. Lower right, the enlarged image containing soma and dendrites with spines.

(H) Grouping of projection neurons based on I:E ratio. Left, example traces show EPSCs (black, $V_{\text{hold}} = -50$ mV) and IPSCs (cyan, $V_{\text{hold}} = 10$ mV) evoked by single optical stimulation of the contralateral BLA afferents. The top and bottom traces represented different cells with the I:E ratio <1 and >1, respectively. Right, summary plots of I:E ratios from the cells with single optical stimulation of the contralateral BLA afferents. Each dot indicates the result of an individual cell. Means \pm SEMs are also shown. Dashed line, I:E ratio = 1.

(I) Pairing of single cortical and single contralateral BLA stimulations. Example traces show postsynaptic potentials (PSPs) evoked by single cortical electrical stimulation (black), single contralateral BLA stimulation (green), and pairing with contralateral BLA optical stimulation (red) at different time intervals (-20, -10, 0, 10, and 20 ms). The top and bottom traces represent different cells with the I:E ratio <1 and >1, respectively.

(J) Summary plots (means \pm SEMs) of the experiments shown in (I). Amplitudes of PSPs evoked by pairing stimulation or cortical stimulation alone at different time intervals are normalized according to the mean PSP calculated from all of the cortical-evoked PSPs at different time intervals. Sample size in (H)-(J): $n = 10$ from 7 mice for I:E ratio <1; $n = 6$ from 5 mice for I:E ratio >1. Wilcoxon matched-pairs signed-rank test was used for comparison between pairing stimulation and cortical stimulation alone at each time interval group in (J).

* $p < 0.05$, ** $p < 0.01$. Scale bars, (A) left and middle, 200 μm , and right, 1,000 μm ; (E) 5 μm ; (F) 100 μm ; (G) left, 200 μm , and lower right, 10 μm .

of contralateral BLA input to BLA PN activity (described below), we re-patched the same or neighboring neurons with a cesium (Cs)-based internal solution and measured the EPSCs and circuit-driven inhibitory postsynaptic currents (IPSCs) upon optical stimulation of the contralateral BLA afferents. We recorded and separately analyzed two groups of neurons: one with weak circuit-driven inhibition (Figure 1H, IPSC versus EPSC, inhibitory:excitatory [I:E] ratio <1), and the other with strong circuit-driven inhibition (Figure 1H, I:E ratio >1). In a separate experiment, input-output curves of contralateral BLA-mediated EPSCs, circuit-driven IPSCs, and I:E ratios versus different light intensities were measured for PNs to further confirm that the strongest light intensity we used in our system can recruit maximal circuit-driven inhibition in both the I:E <1 and >1 groups (Figure S3).

Single stimulation of the contralateral BLA afferents was found to evoke a depolarizing postsynaptic potential (PSP) in both I:E >1 and <1 groups (Figure 1I, green lines). We then investigated whether contralateral BLA afferents have a potentiation or inhibitory effect on other inputs to BLA, such as cortical inputs. To do this, a monopolar electrode was placed on an external capsule to activate the cortical afferents (Figure 1F). Single stimulation of the cortical afferents also evoked a PSP on postsynaptic PNs (Figure 1I, black lines). Paired stimulation of the cortical and contralateral BLA input (Figure 1I, red lines) at the same time (0 ms) or with 20 and 10 ms jittering (−20, −10, 10, and 20 ms) was then performed (Figure 1I, upper panel). We found that no matter whether circuit-driven inhibitions were weak (I:E <1) or strong (I:E >1) and whether contralateral stimulation was applied earlier, later, or simultaneously as cortical stimulation, the amplitude of PSP was further potentiated by paired stimulations compared with cortical input alone (Figures 1I and 1J). The results indicate that contralateral BLA afferents have a potentiation effect on the synaptic activities of BLA PNs.

We then investigated the effect of the contralateral BLA input on repetitive theta-burst frequency stimulation (TBS), a paradigm that mimics physiological theta oscillations (Bazelot et al., 2015; Luo et al., 2011) (Figure 2A). Based on the previously published TBS stimulation paradigm on oChIEF-expressing cells (Bazelot et al., 2015), 10 trains (5 pulses per train at 100 Hz, with 200-ms intervals between trains) of optical TBS consistently induced identical inward currents, and 3 spikes of each train were applied to stimulate BLA (Figure S4). Similarly, contralateral TBS induced either minimized or noticeable circuit-driven inhibition of BLA PNs (Figure 2B). For both I:E <1 and >1 groups, cortical TBS alone generated synaptic depression (Figures 2C–2F, black lines), whereas the contralateral BLA TBS expressed synaptic facilitation (Figures 2C–2F, green lines). Thus, the synaptic dynamics of contralateral connectivity differ from cortical input.

We then used time-locked paired TBS with a 10-ms jittering between cortical and contralateral BLA afferents, a condition mimicking the disynaptic delay and maximizing the effect of circuit-driven inhibition. Compared with cortical TBS alone, the PSPs of paired stimulations were potentiated in both the I:E <1 and >1 groups, particularly for the late PSPs, no matter whether the contralateral BLA TBS was paired before or after the cortical TBS (Figures 2C–2F, red versus black). Moreover, the outcomes of pairing TBS and contralateral BLA TBS alone did not differ in the late stimulus trains (Figures 2C–2F, red versus green). Linear

sum was also comparable to pairing TBS (Figures 2C–2F, blue versus red). Thus, contralateral BLA TBS induces the synaptic facilitation of PSPs, which dominates the synaptic dynamics over the cortical TBS when paired. These results suggest that the potentiation effect of contralateral BLA inputs on PNs also occurs during repetitive stimulation.

Apart from PNs, we also recorded the responses of seven BLA interneurons (Figures S2 and S5). The results of these BLA interneurons were excluded from the above analyses of BLA PNs. We found that, in contrast to the synaptic facilitation recorded in PNs, four of these seven interneurons did not respond to contralateral BLA TBS (Figure S5, interneuron 1 [IN1], IN3, IN4, and IN5) and another two INs actually exhibited synaptic depression (Figure S5, IN2 and IN7). Only one interneuron exhibited synaptic facilitation in response to contralateral BLA TBS (Figure S5, IN6). In the same brain sections in which we recorded interneurons IN2, IN3, IN4, and IN5, we still recorded synaptic facilitation in neighboring BLA PNs (Figure S5). Thus, the same blue light stimulation induced diverse effects on downstream INs compared to PNs, suggesting that the differing responses of PNs and INs are unlikely to be caused by oChIEF properties. Instead, they likely reflect the special synaptic properties of the contralateral BLA afferents.

Involvement of NMDAR in Contralateral BLA Connectivity

The above-described results suggest that the contralateral BLA TBS evokes synaptic facilitation and potentiates cortical TBS input, especially on the late stimulus trains during pairing TBS. We wondered what constitutes the mechanism for this potentiation effect. One possibility is that contralateral BLA TBS itself or pairing TBS of two inputs activate NMDAR by removing the depolarization block of the preceding stimulus. To investigate this possibility, we applied an NMDAR antagonist (D-APV) treatment to our experiments of paired TBS (Figure 3). Since both I:E <1 and >1 groups exhibited similar responses to the contralateral BLA input (Figures 1 and 2), we did not separate these two groups of cells in the following experiments. Similar to the results shown in Figure 2, both contralateral BLA TBS alone and paired stimulation induced synaptic facilitation before adding D-APV (Figures 3A, 3B, 3E, and 3F). In the presence of D-APV, the potentiation effect of contralateral BLA TBS on cortical TBS input was reduced (Figure 3, red lines). For both cortical-contralateral and contralateral-cortical pairing, D-APV treatment reduced the facilitated PSP amplitudes evoked by the contralateral TBS (Figure 3, green lines), as reflected by the reduced delta PSP upon subtracting the initial PSP for the contralateral BLA input alone from the later PSP (Figures 3C and 3G), as well as by a comparison of paired stimulation with cortical input alone (Figures 3D and 3H). These results suggest that NMDAR contributes at least partially to the potentiation of synaptic responses during pairing TBS.

Contralateral BLA Input Also Potentiates the BLA Response to Thalamic Stimulation

In addition to cortical input, we investigated whether the contralateral BLA afferents can modulate ipsilateral thalamic inputs to BLA. The stimulating electrode was placed at the internal capsule to trigger thalamic input and it was paired with the

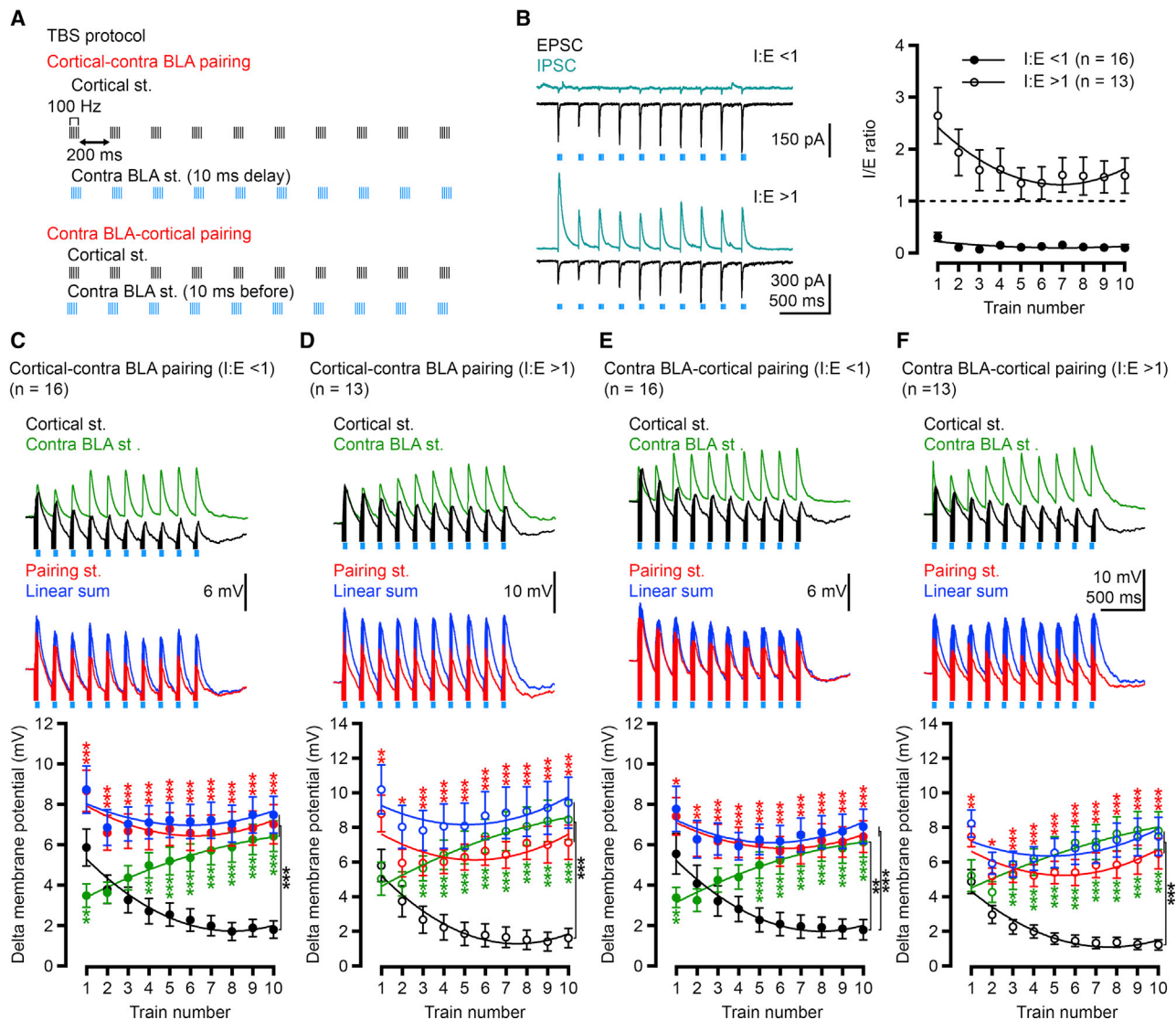


Figure 2. Contralateral BLA Theta-Burst Stimulation (TBS) Expresses Synaptic Facilitation to Potentiate the Synaptic Response of BLA to Cortical TBS

(A) Schematic illustrating TBS of cortical afferents paired with contralateral BLA TBS with a 10-ms jittering.

(B) Similar to Figure 1H, projection neurons were classified based on I:E ratio.

(C–F) Comparison of synaptic dynamics upon TBS of single input or pairing inputs under four different conditions. Contralateral BLA TBS was applied with a 10-ms delay in (C) and (D) or 10 ms beforehand in (E) and (F). The I:E ratio is <1 in (C) and (E) and >1 in (D) and (F). Top: synaptic depression of cortical TBS versus synaptic facilitation of contralateral BLA TBS. Center: comparison of the actual recording of pairing stimulation and linear sum of cortical TBS and contralateral BLA TBS. Example traces show PSPs evoked by different stimulations. Bottom: summary plots (means \pm SEMs) of changes in membrane potentials versus the train number during different stimulations as indicated. Black, electrical TBS of cortical afferents; green, optical TBS of contralateral BLA afferents; red, pairing TBS; blue, predicted linear sum. Sample size in (B)–(F): $n = 16$ from 10 mice for I:E ratio <1 group; $n = 13$ from 10 mice for I:E ratio >1 group. In (C)–(F), two-way repeated-measures ANOVA was used for a comparison of changes in the membrane potentials of different stimulation groups (significance is indicated by black asterisk) with the post hoc Bonferroni’s test to assess the significance at each stimulus train number (green asterisk: cortical st. versus contralateral BLA st.; red asterisk: cortical st. versus pairing st.).

* $p < 0.05$, ** $p < 0.01$, *** $p < 0.001$.

optical stimulation of contralateral BLA afferents (Figure 4A). Paired stimulations of 5 time intervals (–20, –10, 0, 10, and 20 ms) potentiated the synaptic potentials when compared with thalamic stimulation alone (Figures 4B and 4C). During repetitive TBS, thalamic TBS alone also exhibited synaptic depres-

sion (Figures 4D and 4E, black lines), which was a similar outcome to cortical TBS alone (Figures 2 and 3). When we paired thalamic stimulation with contralateral BLA input, no matter whether that meant thalamic-contralateral BLA TBS or contralateral BLA-thalamic pairing TBS, PSPs were potentiated (Figures

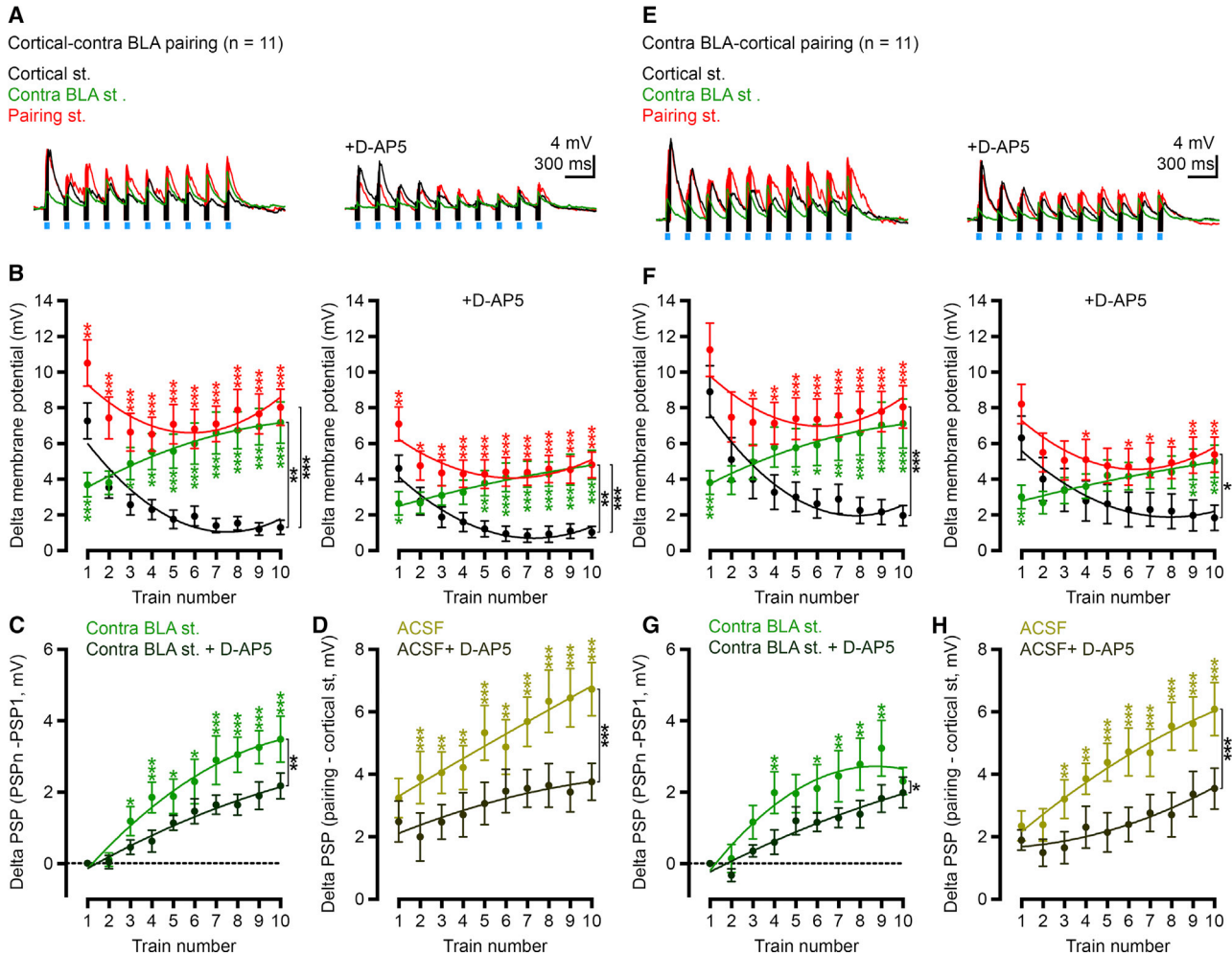


Figure 3. NMDAR Activation Is Involved in Synaptic Facilitation of Contralateral BLA Stimulation

Pairing TBS of contralateral BLA afferents and cortical inputs with a 10-ms jittering was performed as described in Figure 2, except that D-APV treatment was included and that the different I:E ratio was ignored. Black, electrical TBS of cortical afferents; green, optical TBS of contralateral BLA afferents; red, pairing TBS; blue, predicted linear sum.

(A–D) Cortical-contralateral BLA pairing TBS, $n = 11$ from 9 mice. Example traces (A), summary plots (mean \pm SEM) of changes in membrane potentials versus the train number during different stimulations (B), summary plots (means \pm SEMs) of the effect of D-APV treatment on the extent of facilitated PSPs evoked by contralateral BLA TBS (C), summary plots (means \pm SEMs) of the effect of D-APV treatment on the potentiation of PSPs by pairing TBS compared with cortical TBS alone (D).

(E–H) Contralateral BLA-cortical pairing TBS, $n = 11$ from 9 mice. Example traces (E), summary plots (mean \pm SEM) of changes in membrane potentials versus the train number during different stimulations (F), summary plots (means \pm SEMs) of the effect of D-APV treatment on the extent of facilitated PSPs evoked by contralateral BLA TBS (G), summary plots (means \pm SEMs) of the effect of D-APV treatment on the potentiation of PSPs by pairing TBS compared with cortical TBS alone (H).

Two-way repeated-measures ANOVA was used for a statistical comparison of the changes in the membrane potentials of different stimulation groups with the post hoc Bonferroni's test to assess the significance at each stimulus train number. * $p < 0.05$, ** $p < 0.01$, *** $p < 0.001$.

4D and 4E, red versus black). Thus, the interactions of contralateral BLA afferents with thalamic inputs were similar to those with cortical inputs. These results suggest that the potentiation effect of contralateral BLA afferents modulates multiple ipsilateral inputs to BLA.

These *ex vivo* electrophysiological analyses suggest that input from contralateral BLA potentiates and facilitates the synaptic dynamics of the BLA.

c-FOS Expression upon Contralateral Stimulation

Neuronal activation of BLA neurons by contralateral stimulation was further confirmed *in vivo* by c-FOS staining. AAV8-CaMKII-hChR2-eYFP (Yizhar et al., 2011) was unilaterally infected into one BLA (Figure 5). The AAV infection site is referred to as the ipsilateral side, whereas the AAV uninfected site is considered the contralateral side. Ipsilateral activation of hChR2 at the AAV infection site increased the number of c-FOS⁺ cells at

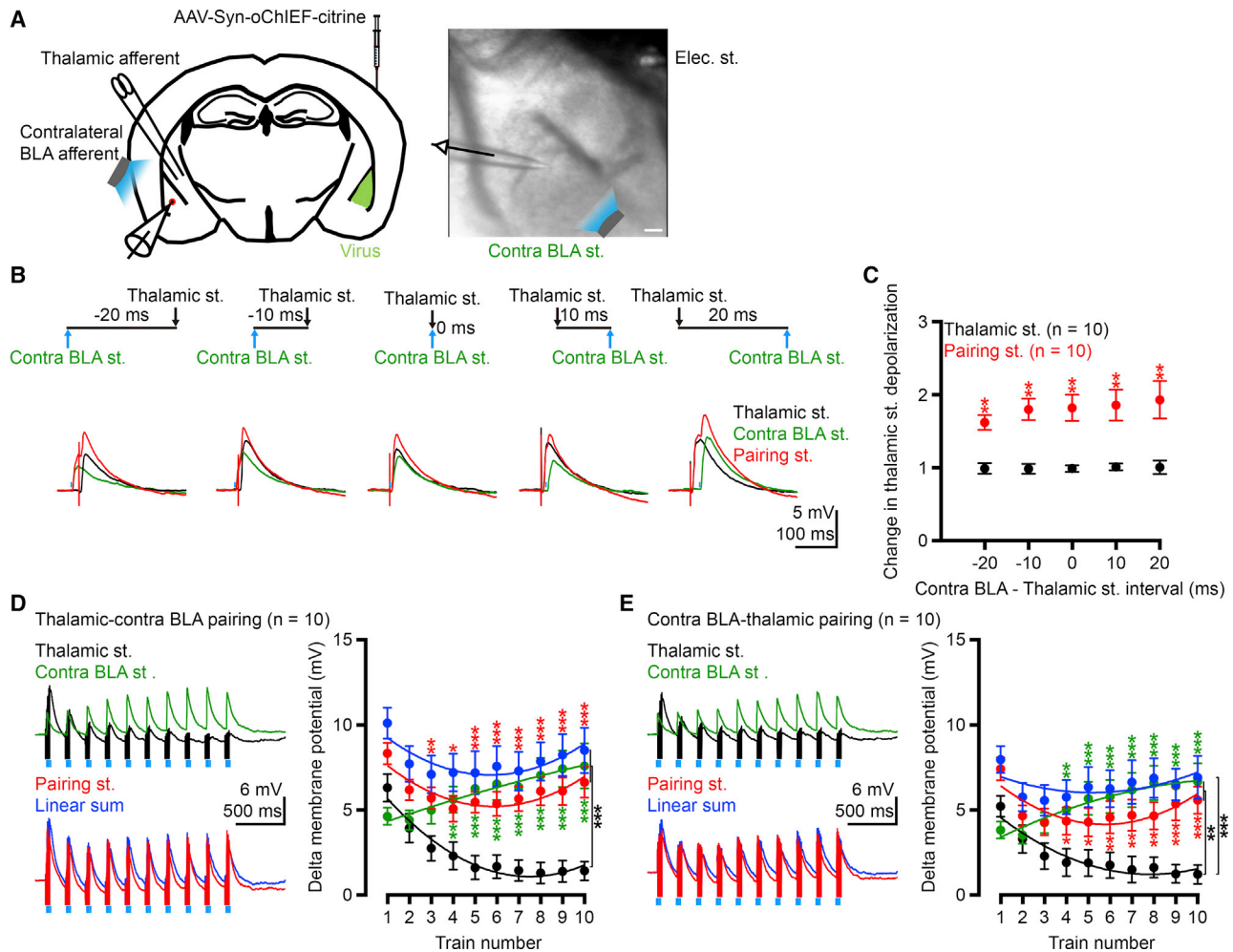


Figure 4. Contralateral BLA Afferents Potentiate Thalamic-BLA Synaptic Responses

Experiments were performed as described in Figures 1 and 2, except that thalamic but not cortical afferents were stimulated. Black, electrical TBS of thalamic afferents; green, optical TBS of contralateral BLA afferents; red, pairing TBS.

(A) Experimental design and IR-DIC image.

(B) Pairing of single thalamic and single contralateral BLA stimulations at different time intervals (–20, –10, 0, 10, and 20 ms).

(C) Summary plots (means ± SEMs) of the experiments shown in (B).

(D) Thalamic-contralateral BLA pairing TBS.

(E) Contralateral BLA-thalamic pairing TBS.

Sample size in (B)–(E): n = 10 from 5 mice. Wilcoxon matched-pairs signed-rank test was used for comparison between pairing stimulation and thalamic stimulation alone at each time interval group in (C). In (D and E), two-way repeated-measures ANOVA was used for a statistical comparison of the changes in membrane potentials of different stimulation groups with post hoc Bonferroni's test to assess the significance at each stimulus train number.

*p < 0.05, **p < 0.01, ***p < 0.001. Scale bar, 100 μm.

contralateral BLA (Figures 5A–5C). When contralateral activation of hChR2 at axonal termini was performed (Figure 5D), the number of c-FOS⁺ BLA cells was also increased upon blue light stimulation (Figures 5E and 5F). Thus, consistent with electrophysiological study, the results of c-FOS staining also suggest that BLA neurons are innervated and activated by contralateral afferents.

We then investigated the properties of neurons activated by contralateral inputs with immunostaining using CaMKII (a PN marker) and GAD67 (an IN marker) (Figures 5G–5I). Similar to the cell population in the BLA (pyramidal neurons ~80% versus

non-pyramidal neurons ~20%) (McDonald, 1982; Tovote et al., 2015), ~78% of neurons were CaMKIIα⁺ and ~15% were GAD67⁺ among c-FOS⁺ cells (Figures 5H and 5I). Thus, contralateral innervation has no specific preference for projection or inhibitory neurons at BLA, which is consistent with the results of our electrophysiological analyses, showing that contralateral BLA stimulation can activate PNs and INs of BLA.

Contralateral Innervation Pattern of BLA

We then wondered how both BLA in the two brain hemispheres innervate each other. To address this question, red retrograde

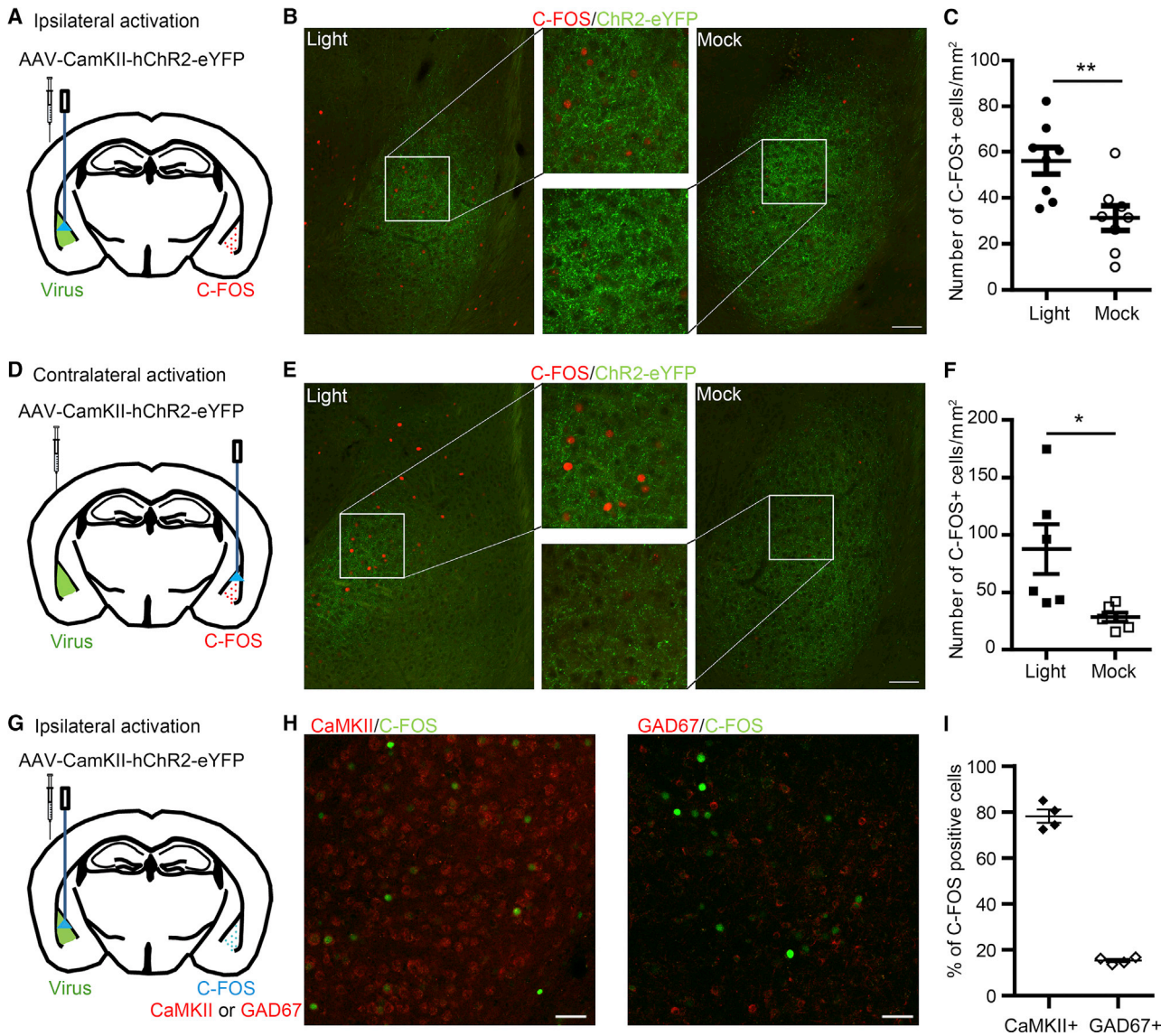


Figure 5. Optogenetic Study Reveals Contralateral Connectivity of the BLA In Vivo

AAV8 was unilaterally infected into the BLA. Two weeks later, blue light stimulation was performed at either the infected site (ipsilateral activation) or at the other BLA (contralateral activation), as indicated. Neural activation in contralateral BLA relative to the AAV infection site was monitored by c-FOS staining. ChR2-eYFP labels the axonal termini of BLA neurons.

(A–C) Ipsilateral activation. Experimental design (A), C-FOS staining (B), and quantification of C-FOS⁺ cells (C) are shown.

(D–F) Contralateral activation. Experimental design (D), C-FOS staining (E), and quantification of C-FOS⁺ cells (F) are shown.

(G–I) Double-staining with c-FOS and CaMKII or GAD67 after ipsilateral activation. Experimental design (G), double staining as indicated (H), and quantification of C-FOS⁺ cells (I) are shown.

* $p < 0.05$, ** $p < 0.01$; unpaired Student's t test. Scale bars, (B) and (E) 100 μm ; (H) 50 μm .

microspheres (hereafter called “red retrobeads”) and AAV-CamKII-hChR2-eYFP were co-injected into the same side of BLAs in the region 1.58–1.82 mm posterior to the bregma, representing the rostral part of amygdalae (before the position at -2 mm related to the bregma). Two weeks later, ipsilateral activation of hChR2-eYFP was performed to examine the distributions of red retrobeads (indicating contralateral projection neurons) and c-FOS immunoreactivities (indicating the cells

directly or indirectly activated by contralateral input) at the contralateral amygdala (Figures 6A, 6B, and S6A). We noticed that red retrobead-positive cells were widely distributed, but were more concentrated at the rostral part of BLA (Figures 6B and S6A), suggesting that rostral parts of both BLA in the two hemispheres tend to innervate each other. In addition, both lateral amygdala (LA) and basal (BA) neurons innervated contralateral BLA, although more BA than LA neurons projected

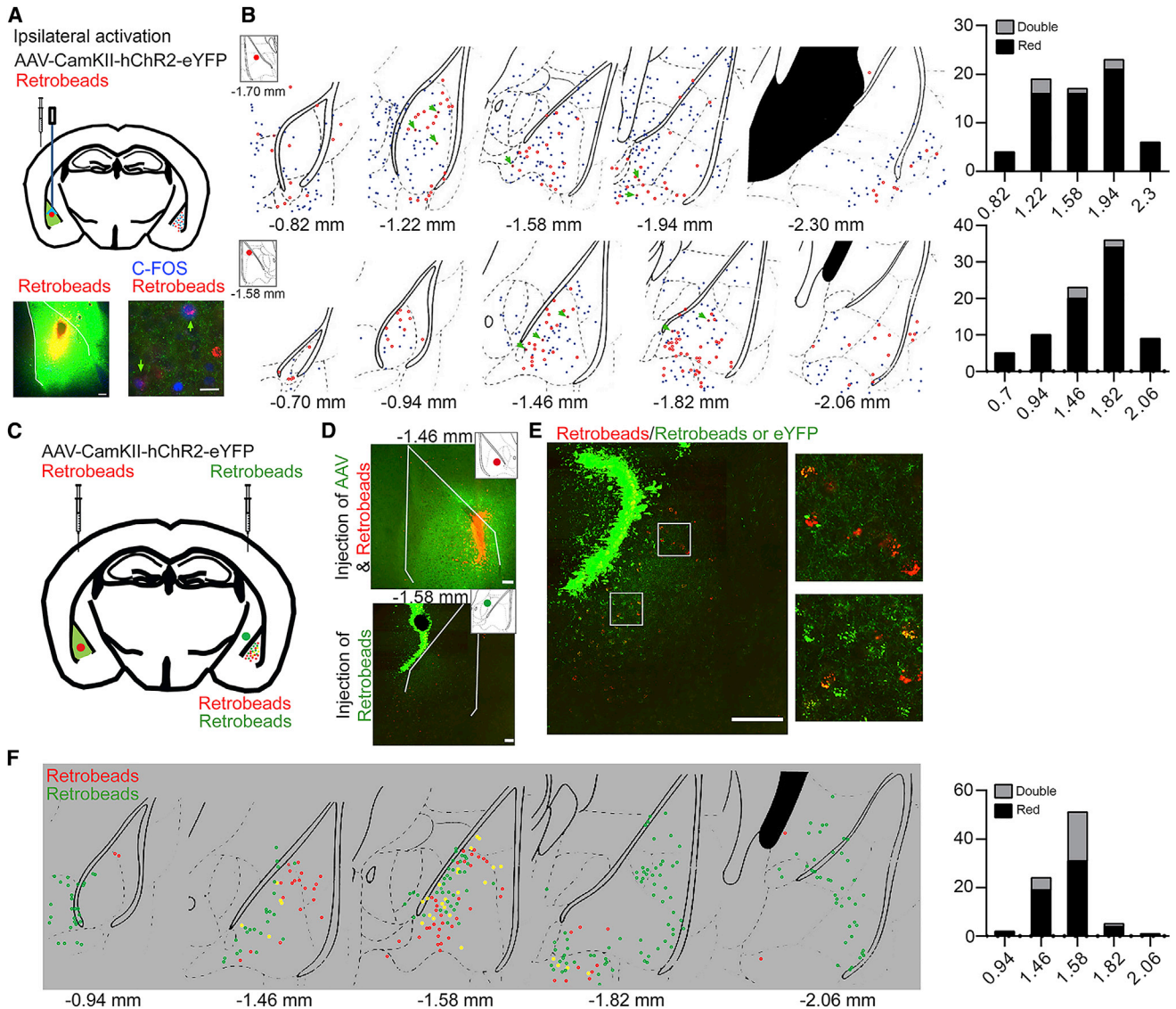


Figure 6. Retrograde Tracing and Contralateral Activation of the BLA

(A and B) Patterns of contralateral afferents and efferents of the BLA.

(A) AAV and red retrobeads were co-injected into one side of the BLA. Two hours after ipsilateral activation with blue light, C-FOS expression and retrobead distribution at the contralateral BLA were examined. Representative images are shown.

(B) Distribution patterns of C-FOS⁺ and red retrobead-positive cells (blue dots and red circles, respectively) at the contralateral side. Green arrows point to double-positive cells. Data on an additional four mice are available in Figure S6A. Insets indicate the injection sites. The rightmost panels show cell numbers of single- and double-positive cells corresponding to the brain sections listed at left.

(C–F) BLA neurons double projecting to the contralateral BLA and ipsilateral CeA.

(C) AAV and red retrobeads were co-injected into one side of the BLA. Green retrobeads were injected into the CeA of the other BLA.

(D) Injection sites of one examined mouse.

(E) Fluorescent image of retrobeads and ChR2-eYFP at the contralateral BLA relative to the AAV infection site. Right, enlarged images.

(F) Distribution patterns of retrobead-positive cells (red and green circles) at the contralateral BLA relative to the red retrobead injection site. Yellow circles indicate double-positive cells. Data on the remaining three mice are available in Figure S6B.

The distance indicates position relative to the bregma. Scale bars, (A, lower left, and D) 100 μ m; (A, lower right) 25 μ m; (E) 200 μ m.

contralaterally under our experimental condition (Figures 6B and S6A). These tracing analyses suggest that BLA neurons located rostrally in the region up to 2 mm posterior to the bregma widely innervate to contralateral BLA, but they still have their own tar-

geting preference, and the innervation pattern is not completely random.

The contralateral efferent targets indicated by c-FOS immunoreactivities were also widely distributed from the rostral to the

caudal parts of the amygdalae (Figures 6B and S6A). We noticed that red retrobeads and c-FOS immunoreactivities were mainly segregated in different cells (Figures 6B and S6A). Of the 30 brain sections we prepared from 6 mice, only 38 c-FOS and red retrobead double-positive cells were identified from a total of 815 c-FOS⁺ cells and 424 red retrobead-positive cells (Figures 6B and S6A; green arrows point to double-positive cells). Therefore, only ~9% of red retrobead-positive cells were also c-FOS⁺. Thus, contralateral afferent and efferent neurons of a given BLA neuron tend to be different. Reciprocally activated BLA neurons accounted for a small population of neurons at the rostral part of BLA.

Dual Projection of BLA Neurons to Ipsilateral CeA and Contralateral BLA

We then wondered whether a single BLA neuron is capable of projecting to both the contralateral BLA and the ipsilateral CeA. Red retrobeads and AAV8-ChR2-eYFP were co-injected into the contralateral BLA, whereas green retrobeads were injected into the ipsilateral CeA (Figures 6C and 6D). Although the emission wavelength of eYFP overlaps significantly with green retrobeads, these two signals could still be distinguished based on distribution patterns; green retrobeads were bright puncta located in soma, whereas eYFP outlined filamentous axonal shafts and termini (Figure 6E). Since it is unclear how dual-projecting BLA neurons innervate contralaterally and ipsilaterally and since retrobead labeling is restricted to a population of neurons that extend their axons to the retrobead implantation region, we endeavored to implant retrobeads at slightly different positions and then examined whether we could identify green and red retrobead double-positive cells at BLA. In the two mice we examined, red retrobeads were injected into contralateral BLA at a position -1.46 mm relative to the bregma and green retrobeads were implanted in the ipsilateral CeA at positions -1.58 and -1.46 mm relative to the bregma, respectively. We identified 26 or 18 double-positive cells in these mice (Figures 6F and S6B, upper panel). In another two mice, retrobeads were placed at positions -1.7 mm versus -1.46 mm (representing contralateral BLA versus ipsilateral CeA) or -1.22 mm versus -1.7 mm relative to the bregma, respectively, but only 0 or 4 double-positive cells were found (Figure S6B, center and bottom). Accordingly, these dual-projection neurons seem to preferentially innervate the contralateral BLA and ipsilateral CeA located at approximately the same distance from the bregma, such as -1.46 mm versus -1.46 mm (Figure S6B, upper) or -1.46 mm versus -1.58 mm (Figures 6D–6F). Thus, the innervation pattern of BLA to contralateral BLA and ipsilateral CeA is not random. Since retrobeads were placed locally at BLA and CeA, our analysis was not expected to identify all of the dual-projection neurons and, consequently, the population of dual-projection neurons is underestimated under our experimental conditions.

Unilateral Inhibition of BLA Bilaterally Reduces BLA Activity and Impairs Social Behavior and Memory

We then used two behavioral assays, reciprocal social interaction and conditioned taste aversion, in combination with two treatments, pharmacological inhibition and chemogenetic disconnection, to evaluate the role of contralateral connectivity

in BLA. Reciprocal social interaction is a task used to assess the free social interactions of test mice with strangers. Conditioned taste aversion is used to analyze amygdala-dependent associative memory. After conditioning sucrose solution availability with an aversion response, control mice learned that sucrose solution may not be a safe food. Consequently, these control mice exhibited reduced drinking amounts of sucrose solution in a subsequent two-bottle assay in which water and sucrose solution were provided simultaneously. If contralateral input is indeed critical for the full activation of amygdalae, then we expected that unilateral inhibition of amygdalar activity or disconnection of contralateral BLA input would be sufficient to impair mouse performance in reciprocal social interaction and conditioned taste aversion, both of which require normal amygdalar activity and function.

In the first set of experiments, the neuronal activity of one BLA was locally reduced using ifenprodil, an inhibitor of NMDAR2B, since glutamate receptor-dependent plasticity is required for amygdala-dependent memory (Bauer et al., 2002; Kim et al., 1991; Miserendino et al., 1990; Rumpel et al., 2005). Ifenprodil was randomly injected into either the right or left BLA to unilaterally inhibit BLA activity (Figure 7A). We first used reciprocal social interaction to assess the free interaction of test mice with strangers. Compared with vehicle controls, unilaterally ifenprodil-treated mice exhibited a reduced reciprocal social interaction (Figure 7B), suggesting that unilateral inhibition of one BLA is sufficient to reduce the sociability of mice. In conditioned taste aversion, unilateral ifenprodil treatment did not influence the sucrose preference of mice at training day (Figure 7C, left). After conditioning sucrose solution availability with an aversion response, ifenprodil-treated mice drank more sucrose solution than did control mice in a two-bottle sucrose memory test (Figure 7C, right), indicating impaired associative memory in conditioned taste aversion. c-FOS expression also indicated that the unilateral infusion of ifenprodil was sufficient to reduce neuronal activation at both BLAs (Figure 7D). Our results suggest that the unilateral inactivation of an amygdala is sufficient to disrupt amygdala function.

BLA Impairment by Chemogenetic Disconnection of Contralateral Stimulation

We next performed chemogenetic disconnection (Stachniak et al., 2014) to further evaluate the function of contralateral BLA stimulation. The silencing effect of hM4D on contralateral BLA axons was first confirmed by slice recording. AAV8-hM4D(Gi)-mCherry and AAV8-Syn-oChIEF-citrine were co-injected into one BLA (Figure 7E). Whole-cell current-clamp recording on the contralateral BLA PN was performed to demonstrate that the batch application of clozapine-N-oxide (CNO, an agonist of hM4D) rapidly inhibited the light-evoked PSP in contralateral BLA PN (Figures 7F and 7G), suggesting the silencing efficacy of hM4D on contralateral BLA axonal termini.

To investigate the function of BLA contralateral stimulation in mouse behaviors, AAV8-hM4D(Gi)-mCherry and AAV8-ChR2-eYFP as a negative control were randomly injected into either the right or left BLA. Thirty minutes before mice underwent behavioral tasks, CNO was locally infused into the uninfected BLA to suppress the neurotransmission of contralateral BLA

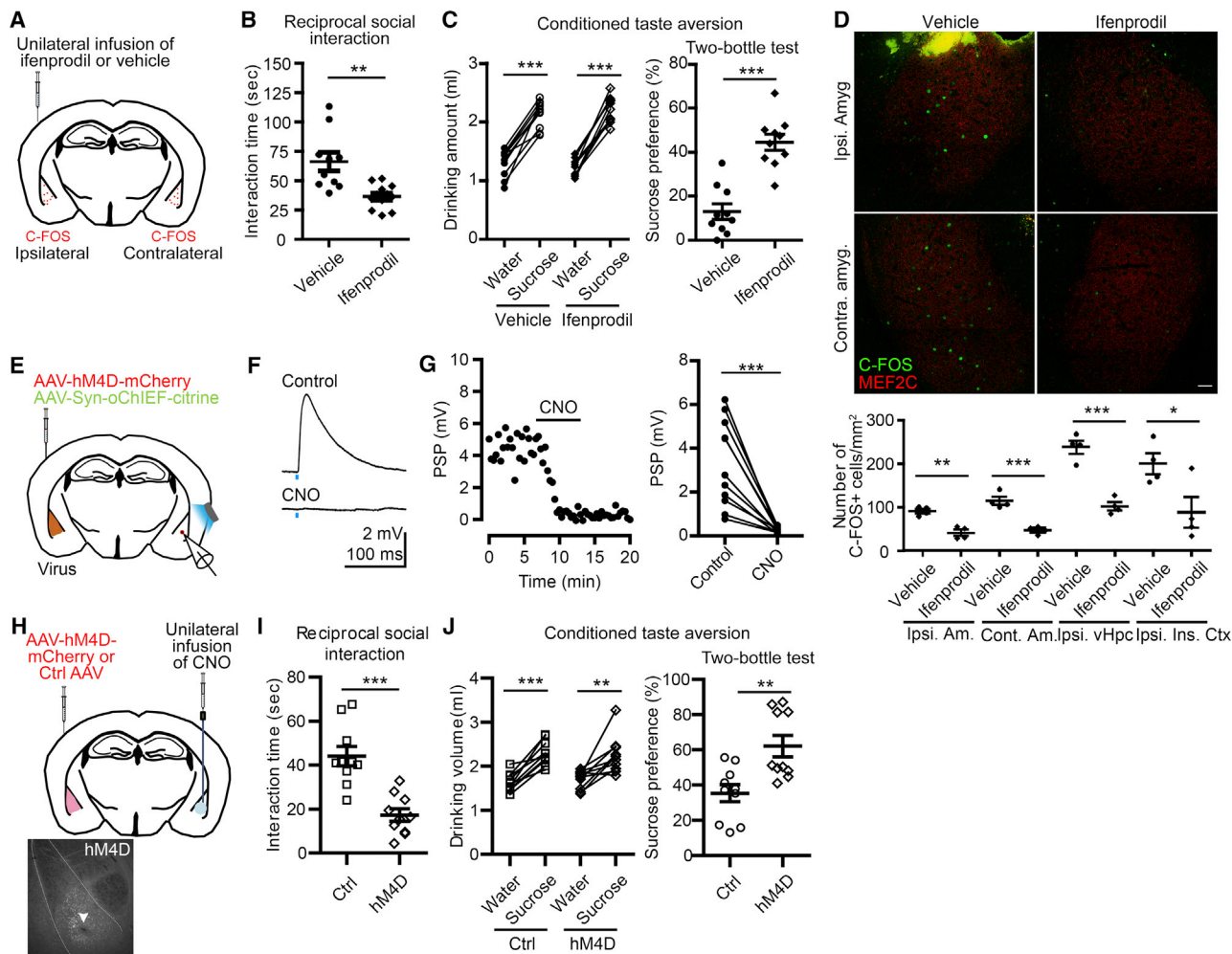


Figure 7. Amygdalar Impairment by Unilateral Inhibition of the BLA

(A–D) Unilateral injection of ifenprodil inhibits the function and activation of BLA.

(A) Unilateral injection at either the left or right BLA.

(B) Reciprocal social interaction.

(C) Conditioned taste aversion. Left, amounts of water drunk 1 day before training and of sucrose solution on the training day. Right, sucrose preference in a two-bottle sucrose memory test.

(D) Double immunostaining with c-FOS and MEF2C (to outline the BLA) antibodies 2 h after the conditioned taste aversion and quantification of c-FOS⁺ cells in BLA, ipsilateral ventral hippocampus, and ipsilateral insular cortex.

(E–G) Slice recording was used to validate the silencing efficacy of hM4D on contralateral BLA axons.

(E) Experimental design.

(F) Light-evoked PSP in BLA PN before and after bath application of CNO (5 μ M). The traces are averages of 10 sweeps for each condition.

(G) Left: time course for the experiment shown in (F). Right: summary plots of the effects of CNO on light-evoked PSP. n = 11 from 6 mice.

(H–J) Chemogenetic disconnection of contralateral BLA activities impairs amygdala-dependent behaviors.

(H) Experimental design. Two weeks after AAV injection, CNO was locally infused into the contralateral BLA. Thirty minutes later, mice were subjected to behavioral analyses.

(I) Reciprocal social interaction.

(J) Conditioned taste aversion.

In (B)–(D), (I), and (J), each dot indicates the result of an individual mouse. Means \pm SEMs are also shown.

*p < 0.05, **p < 0.01, ***p < 0.001; unpaired Student's t test (for B, I, lower panel of D, and right panels of C and J); paired Student's t test (for left panels of C and J). Wilcoxon matched-pairs signed rank test was used for the right panel of (G). Scale bar, 50 μ m.

axonal termini (Figure 7H). We found that unilateral administration of CNO effectively reduced the interaction time of hM4D-expressing mice in reciprocal social interaction but not that of control mice (Figure 7I), suggesting that the disconnection of

contralateral BLA connectivity impairs social interaction. In conditioned taste aversion, these hM4D-expressing mice still exhibited a sucrose preference at training day (Figure 7J, left). The hM4D-expressing group drank more sucrose solution in a

two-bottle sucrose memory test (Figure 7J, right), suggesting that the disruption of contralateral BLA connectivity impairs the memory of conditioned taste aversion. Our results indicate that contralateral connectivity is critical for amygdala-dependent activity and function.

DISCUSSION

In this report, electrophysiological, optogenetic, and tracing studies suggest that contralateral innervation between both BLA in the brain potentiates and facilitates the synaptic responses of BLA neurons. Contralateral potentiation and facilitation mutually enhance and synchronize BLA activity in the two brain hemispheres. Pharmacological and chemogenetic inhibition further support that contralateral facilitation is critical for amygdala-dependent behaviors. Our results suggest that mutual contralateral potentiation of BLA is required for the full activation and functionality of BLA and is critical for social interaction and associative memory.

Our results suggest that mutual activation between both BLA of the two brain hemispheres intensifies an essential neural circuit to amplify the signal in BLA for triggering downstream information processing. In this scenario, any interference in this mutual amplification circuitry, such as via unilateral inhibition with a pharmacologic treatment (chemogenetic disconnection of contralateral BLA input), will impair BLA-dependent functioning. Our study also provides a mechanism explaining the previous findings that the unilateral inhibition of BLA is sufficient to disrupt amygdala function (Chaudhri et al., 2013; Coleman-Meschers et al., 1996; Gilmartin et al., 2012) and explains how the impairment of neuronal activation in 10%–20% of BLA neurons is sufficient to reduce amygdala-dependent memory (Rumpel et al., 2005).

Although BLA contralateral connectivity potentiates BLA synaptic responses, interhemispheric inhibition is common in other brain regions. For example, motor and somatosensory cortical areas send transcallosal axons to contralateral homotopic regions and preferentially activate inhibitory neurons (Meyer et al., 1995; Palmer et al., 2012). In the hippocampus, hilar mossy cells send commissural axons through the hippocampal commissure to target the contralateral dentate gyrus. The hilar commissural inputs also preferentially recruit a subset of INs to suppress granule cell spiking (Buzsàki and Eidelberg, 1981; Hsu et al., 2016). Interhemispheric inhibition mediated by hilar commissural inputs is important for spatial memory and to prevent runaway excitations of granule cells (Bui et al., 2018). Thus, depending on the properties of contralateral PNs, the effects of different contralateral connectivity vary.

It has been reported that BLA neurons display intrinsic theta oscillations upon prolonged depolarizing stimuli (Pape and Driessang, 1998; Paré et al., 1995), which contribute to rhythmic firing activities. Local field potential recordings on awake animals further revealed the synchronized theta or theta-fast gamma coupling oscillations in the BLA, medial prefrontal cortex, and ventral hippocampus during fear memory retrieval (Karalis et al., 2016; Stujenske et al., 2014). In our study, we used paired TBS of contralateral BLA afferents with cortical or thalamic inputs to mimic synchronized theta oscillations. In contrast to

the synaptic depression of cortical afferents and thalamic afferents, BLA contralateral synaptic input on BLA PNs features synaptic facilitation. This facilitating feature of synaptic activities suggests that contralateral BLA activities are important for theta oscillation-related spike coding, which has been investigated in hippocampal theta oscillations for its roles in phase precession (Thurley et al., 2008) and the possible short-term memory buffering ability that converts slow behavioral temporal correlation into rapid changes in neuronal dynamics (Leibold et al., 2008). These kinds of synaptic responses induced by contralateral BLA TBS are different from those evoked by ventral hippocampus TBS, which induces synaptic depression and recruits INs to inhibit BLA PN spiking (Bazelot et al., 2015). Although circuit-driven inhibition can be induced by contralateral BLA afferents, it does not seem to impair the facilitating effect of contralateral BLA afferents on the PSPs of BLA PNs either by single pulse or TBS (Figures 1 and 2). Contralateral BLA afferents induce the diverse synaptic dynamics of BLA INs (Figure S5). Thus, the facilitation effect of contralateral BLA afferents on BLA PNs is unlikely to be due to the manipulation of optogenetic stimulation. Apart from contralateral innervation, BLA afferents to ipsilateral CeA also exhibit synaptic facilitation (Watabe et al., 2013). Thus, synaptic facilitation may not be unique for BLA contralateral connectivity. It is likely a general feature of some BLA outputs.

Our retrograde tracing analysis shows that projections of a single BLA neuron to both contralateral BLA and ipsilateral CeA are possible. The projection pattern of double-projection neuron revealed a regional preference, focused on a region approximately the same distance from the bregma. Thus, the geographic distribution of a given double-projection BLA neuron and its innervating targets is not random. In addition, our data suggest that for BLA neurons, their contralateral afferent PNs and contralateral efferent neurons tended to be different. It will be interesting to explore further how contralateral connectivity between BLA integrates with other afferents and efferents of BLA.

Homotopic interhemispheric connectivity, which links the same brain regions in the two hemispheres, is the most robust subset of brain connectivity, showing a difference between patients with ASD and matched controls (Anderson et al., 2011; Dinstein et al., 2011; Hahamy et al., 2015; Khan et al., 2013; Orekhova et al., 2014). Our analysis of contralateral BLA connectivity provides a model explaining how interhemispheric long-range connectivity controls brain activity and function and strengthens the evidence for the critical role of interhemispheric connectivity in responses to environmental stimulation.

STAR★METHODS

Detailed methods are provided in the online version of this paper and include the following:

- KEY RESOURCES TABLE
- LEAD CONTACT AND MATERIALS AVAILABILITY
- EXPERIMENTAL MODEL AND SUBJECT DETAILS
- METHOD DETAILS
 - Production of pseudotyped AAV8 vectors
 - Stereotaxic surgery, probe implantation and injection of AAV and retrograde microbeads

- Optogenetic stimulation for C-FOS staining
- Chemogenetic study
- Slice electrophysiology
- Immunofluorescence staining
- Confocal microscopy, imaging, and Imaris 3D construction
- Behavioral analyses
- Pharmacological treatment
- **QUANTIFICATION AND STATISTICAL ANALYSIS**
- **DATA AND CODE AVAILABILITY**

SUPPLEMENTAL INFORMATION

Supplemental Information can be found online at <https://doi.org/10.1016/j.celrep.2019.08.082>.

ACKNOWLEDGMENTS

We thank Dr. Cheng-Chang Lien for assistance related to the optogenetic study; the AAV core facility of the Institute of Biomedical Science; the Neuroscience core facility (supported by grant no. AS-CFII-108-106); the animal facility, the imaging core, and the transgenic core facility of the Institute of Molecular Biology, Academia Sinica, for equipment and technical assistance; Dr. Karl Deisseroth for AAV-CaMKII α -hChR2(C128S/D156A)-eYFP (Addgene plasmid #35501) and AAV-CaMKII α -hChR2(H134R)-eYFP; Dr. Bryan Roth for AAV-CaMKII α -hM4D(Gi)-mCherry (Addgene #50477-AAV8); Dr. John O'Brien for English language editing; and members of the laboratory of Y.-P.H. for relabeling the samples for the blind experiments. This work was supported by grants from Academia Sinica (AS-IA-106-L04) and the Ministry of Science and Technology (MOST 108-2321-B-001-002 and 105-2311-B-001-061-MY3) to Y.-P.H. and the National Health and Medical Research Council, Australia (NHMRC 1103034), to J.Y.L.

AUTHOR CONTRIBUTIONS

T.-N.H. designed and performed the tracing experiments, the c-FOS staining, chemogenetics, and behavioral assays and wrote the manuscript. T.-T.H. designed, performed, assembled, and analyzed all of the electrophysiological recording experiments and wrote the manuscript. H.-C.C. designed and performed the pharmaceutical inhibition experiments and wrote the manuscript. M.-H.L. performed the axon tracing and image processing and wrote the manuscript. H.-T.H. carried out the image processing and wrote the manuscript. C.-P.S. and M.-H.T. prepared AAV. J.Y.L. provided the viral constructs and wrote the manuscript. Y.-P.H. performed the project planning and design, writing of the manuscript, and secured funding support.

DECLARATION OF INTERESTS

The authors declare no competing interests.

Received: March 4, 2019

Revised: July 30, 2019

Accepted: August 26, 2019

Published: October 1, 2019

REFERENCES

Aboitiz, F., and Montiel, J. (2003). One hundred million years of interhemispheric communication: the history of the corpus callosum. *Braz. J. Med. Biol. Res.* *36*, 409–420.

Anderson, J.S., Nielsen, J.A., Froehlich, A.L., DuBray, M.B., Druzgal, T.J., Carliello, A.N., Cooperrider, J.R., Zielinski, B.A., Ravichandran, C., Fletcher, P.T., et al. (2011). Functional connectivity magnetic resonance imaging classification of autism. *Brain* *134*, 3742–3754.

Arnone, D., McIntosh, A.M., Tan, G.M., and Ebmeier, K.P. (2008). Meta-analysis of magnetic resonance imaging studies of the corpus callosum in schizophrenia. *Schizophr. Res.* *101*, 124–132.

Bauer, E.P., Schafe, G.E., and LeDoux, J.E. (2002). NMDA receptors and L-type voltage-gated calcium channels contribute to long-term potentiation and different components of fear memory formation in the lateral amygdala. *J. Neurosci.* *22*, 5239–5249.

Bazelot, M., Bocchio, M., Kasugai, Y., Fischer, D., Dodson, P.D., Ferraguti, F., and Capogna, M. (2015). Hippocampal Theta Input to the Amygdala Shapes Feedforward Inhibition to Gate Heterosynaptic Plasticity. *Neuron* *87*, 1290–1303.

Bui, A.D., Nguyen, T.M., Limouse, C., Kim, H.K., Szabo, G.G., Felong, S., Maroso, M., and Soltesz, I. (2018). Dentate gyrus mossy cells control spontaneous convulsive seizures and spatial memory. *Science* *359*, 787–790.

Bulfone, A., Smiga, S.M., Shimamura, K., Peterson, A., Puelles, L., and Rubenstein, J.L. (1995). T-brain-1: a homolog of Brachyury whose expression defines molecularly distinct domains within the cerebral cortex. *Neuron* *15*, 63–78.

Bulfone, A., Wang, F., Hevner, R., Anderson, S., Cutforth, T., Chen, S., Menezes, J., Pedersen, R., Axel, R., and Rubenstein, J.L. (1998). An olfactory sensory map develops in the absence of normal projection neurons or GABAergic interneurons. *Neuron* *21*, 1273–1282.

Buzsáki, G., and Eidelberg, E. (1981). Commissural projection to the dentate gyrus of the rat: evidence for feed-forward inhibition. *Brain Res.* *230*, 346–350.

Chaudhri, N., Woods, C.A., Sahuque, L.L., Gill, T.M., and Janak, P.H. (2013). Unilateral inactivation of the basolateral amygdala attenuates context-induced renewal of Pavlovian-conditioned alcohol-seeking. *Eur. J. Neurosci.* *38*, 2751–2761.

Chen, C.C., Sun, C.P., Ma, H.I., Fang, C.C., Wu, P.Y., Xiao, X., and Tao, M.H. (2009). Comparative study of anti-hepatitis B virus RNA interference by double-stranded adeno-associated virus serotypes 7, 8, and 9. *Mol. Ther.* *17*, 352–359.

Chuang, H.C., Huang, T.N., and Hsueh, Y.P. (2014). Neuronal excitation upregulates Tbr1, a high-confidence risk gene of autism, mediating Grin2b expression in the adult brain. *Front. Cell. Neurosci.* *8*, 280.

Chuang, H.C., Huang, T.N., and Hsueh, Y.P. (2015). T-Brain-1—A Potential Master Regulator in Autism Spectrum Disorders. *Autism Res.* *8*, 412–426.

Chung, W.C., Huang, T.N., and Hsueh, Y.P. (2011). Targeted deletion of CASK-interacting nucleosome assembly protein causes higher locomotor and exploratory activities. *Neurosignals* *19*, 128–141.

Coleman-Meschers, K., Salinas, J.A., and McGaugh, J.L. (1996). Unilateral amygdala inactivation after training attenuates memory for reduced reward. *Behav. Brain Res.* *77*, 175–180.

De Rubeis, S., He, X., Goldberg, A.P., Poultney, C.S., Samocha, K., Cicek, A.E., Kou, Y., Liu, L., Fromer, M., Walker, S., et al.; DDD Study; Homozygosity Mapping Collaborative for Autism; UK10K Consortium (2014). Synaptic, transcriptional and chromatin genes disrupted in autism. *Nature* *515*, 209–215.

Dhar, M., Been, P.H., Minderaa, R.B., and Althaus, M. (2010). Reduced inter-hemispheric coherence in dyslexic adults. *Cortex* *46*, 794–798.

Dinstein, I., Pierce, K., Eyster, L., Solso, S., Malach, R., Behrmann, M., and Courchesne, E. (2011). Disrupted neural synchronization in toddlers with autism. *Neuron* *70*, 1218–1225.

Fenlon, L.R., and Richards, L.J. (2015). Contralateral targeting of the corpus callosum in normal and pathological brain function. *Trends Neurosci.* *38*, 264–272.

Ferreira, G., Miranda, M.I., De la Cruz, V., Rodríguez-Ortiz, C.J., and Bermúdez-Rattoni, F. (2005). Basolateral amygdala glutamatergic activation enhances taste aversion through NMDA receptor activation in the insular cortex. *Eur. J. Neurosci.* *22*, 2596–2604.

Frazier, T.W., and Hardan, A.Y. (2009). A meta-analysis of the corpus callosum in autism. *Biol. Psychiatry* *66*, 935–941.

Geschwind, D.H., and Levitt, P. (2007). Autism spectrum disorders: developmental disconnection syndromes. *Curr. Opin. Neurobiol.* *17*, 103–111.

- Gilmartin, M.R., Kwapis, J.L., and Helmstetter, F.J. (2012). Trace and contextual fear conditioning are impaired following unilateral microinjection of muscimol in the ventral hippocampus or amygdala, but not the medial prefrontal cortex. *Neurobiol. Learn. Mem.* *97*, 452–464.
- Hahamy, A., Behrmann, M., and Malach, R. (2015). The idiosyncratic brain: distortion of spontaneous connectivity patterns in autism spectrum disorder. *Nat. Neurosci.* *18*, 302–309.
- Hevner, R.F., Shi, L., Justice, N., Hsueh, Y., Sheng, M., Smiga, S., Bulfone, A., Goffinet, A.M., Campagnoni, A.T., and Rubenstein, J.L. (2001). *Tbr1* regulates differentiation of the preplate and layer 6. *Neuron* *29*, 353–366.
- Hsu, T.T., Lee, C.T., Tai, M.H., and Lien, C.C. (2016). Differential Recruitment of Dentate Gyrus Interneuron Types by Commissural Versus Perforant Pathways. *Cereb. Cortex* *26*, 2715–2727.
- Huang, T.N., and Hsueh, Y.P. (2017). Calcium/calmodulin-dependent serine protein kinase (CASK), a protein implicated in mental retardation and autism-spectrum disorders, interacts with T-Brain-1 (TBR1) to control extinction of associative memory in male mice. *J. Psychiatry Neurosci.* *42*, 37–47.
- Huang, T.N., Chuang, H.C., Chou, W.H., Chen, C.Y., Wang, H.F., Chou, S.J., and Hsueh, Y.P. (2014). *Tbr1* haploinsufficiency impairs amygdalar axonal projections and results in cognitive abnormality. *Nat. Neurosci.* *17*, 240–247.
- Huang, T.N., Yen, T.L., Qiu, L.R., Chuang, H.C., Lerch, J.P., and Hsueh, Y.P. (2019). Haploinsufficiency of autism causative gene *Tbr1* impairs olfactory discrimination and neuronal activation of the olfactory system in mice. *Mol. Autism* *10*, 5.
- Janak, P.H., and Tye, K.M. (2015). From circuits to behaviour in the amygdala. *Nature* *517*, 284–292.
- Jouandret, M.L., and Hartenstein, V. (1983). Basal telencephalic origins of the anterior commissure of the rat. *Exp. Brain Res.* *50*, 183–192.
- Karalis, N., Dejean, C., Chaudun, F., Khoder, S., Rozeske, R.R., Wurtz, H., Bagur, S., Benchenane, K., Sirota, A., Courtin, J., and Herry, C. (2016). 4-Hz oscillations synchronize prefrontal-amygdala circuits during fear behavior. *Nat. Neurosci.* *19*, 605–612.
- Khan, S., Gramfort, A., Shetty, N.R., Kitzbichler, M.G., Ganesan, S., Moran, J.M., Lee, S.M., Gabrieli, J.D., Tager-Flusberg, H.B., Joseph, R.M., et al. (2013). Local and long-range functional connectivity is reduced in concert in autism spectrum disorders. *Proc. Natl. Acad. Sci. USA* *110*, 3107–3112.
- Kim, J.J., DeCola, J.P., Landeira-Fernandez, J., and Fanselow, M.S. (1991). N-methyl-D-aspartate receptor antagonist APV blocks acquisition but not expression of fear conditioning. *Behav. Neurosci.* *105*, 126–133.
- LeDoux, J.E., Moscarello, J., Sears, R., and Campese, V. (2017). The birth, death and resurrection of avoidance: a reconceptualization of a troubled paradigm. *Mol. Psychiatry* *22*, 24–36.
- Lee, J.H., Durand, R., Gradinaru, V., Zhang, F., Goshen, I., Kim, D.S., Fenno, L.E., Ramakrishnan, C., and Deisseroth, K. (2010). Global and local fMRI signals driven by neurons defined optogenetically by type and wiring. *Nature* *465*, 788–792.
- Lee, E.J., Lee, H., Huang, T.N., Chung, C., Shin, W., Kim, K., Koh, J.Y., Hsueh, Y.P., and Kim, E. (2015). Trans-synaptic zinc mobilization improves social interaction in two mouse models of autism through NMDAR activation. *Nat. Commun.* *6*, 7168.
- Leibold, C., Gundlfinger, A., Schmidt, R., Thurley, K., Schmitz, D., and Kempfer, R. (2008). Temporal compression mediated by short-term synaptic plasticity. *Proc. Natl. Acad. Sci. USA* *105*, 4417–4422.
- Lin, J.Y. (2013). Production and validation of recombinant adeno-associated virus for channelrhodopsin expression in neurons. *Methods Mol. Biol.* *998*, 401–415.
- Lin, J.Y., Lin, M.Z., Steinbach, P., and Tsien, R.Y. (2009). Characterization of engineered channelrhodopsin variants with improved properties and kinetics. *Biophys. J.* *96*, 1803–1814.
- Lindwall, C., Fothergill, T., and Richards, L.J. (2007). Commissure formation in the mammalian forebrain. *Curr. Opin. Neurobiol.* *17*, 3–14.
- Luo, A.H., Tahsili-Fahadan, P., Wise, R.A., Lupica, C.R., and Aston-Jones, G. (2011). Linking context with reward: a functional circuit from hippocampal CA3 to ventral tegmental area. *Science* *333*, 353–357.
- McDonald, A.J. (1982). Neurons of the lateral and basolateral amygdaloid nuclei: a Golgi study in the rat. *J. Comp. Neurol.* *212*, 293–312.
- Meyer, B.U., Röricht, S., Gräfin von Einsiedel, H., Kruggel, F., and Weindl, A. (1995). Inhibitory and excitatory interhemispheric transfers between motor cortical areas in normal humans and patients with abnormalities of the corpus callosum. *Brain* *118*, 429–440.
- Miranda, M.I., and McGaugh, J.L. (2004). Enhancement of inhibitory avoidance and conditioned taste aversion memory with insular cortex infusions of 8-Br-cAMP: involvement of the basolateral amygdala. *Learn Mem.* *11*, 312–317.
- Miserendino, M.J., Sananes, C.B., Melia, K.R., and Davis, M. (1990). Blocking of acquisition but not expression of conditioned fear-potentiated startle by NMDA antagonists in the amygdala. *Nature* *345*, 716–718.
- Nawaratne, V., Leach, K., Suratman, N., Loiacono, R.E., Felder, C.C., Ambruster, B.N., Roth, B.L., Sexton, P.M., and Christopoulos, A. (2008). New insights into the function of M4 muscarinic acetylcholine receptors gained using a novel allosteric modulator and a DREADD (designer receptor exclusively activated by a designer drug). *Mol. Pharmacol.* *74*, 1119–1131.
- Neale, B.M., Kou, Y., Liu, L., Ma'ayan, A., Samocha, K.E., Sabo, A., Lin, C.F., Stevens, C., Wang, L.S., Makarov, V., et al. (2012). Patterns and rates of exonic de novo mutations in autism spectrum disorders. *Nature* *485*, 242–245.
- O’Roak, B.J., Vives, L., Fu, W., Egertson, J.D., Stanaway, I.B., Phelps, I.G., Carvill, G., Kumar, A., Lee, C., Ankenman, K., et al. (2012a). Multiplex targeted sequencing identifies recurrently mutated genes in autism spectrum disorders. *Science* *338*, 1619–1622.
- O’Roak, B.J., Vives, L., Girirajan, S., Karakoc, E., Krumm, N., Coe, B.P., Levy, R., Ko, A., Lee, C., Smith, J.D., et al. (2012b). Sporadic autism exomes reveal a highly interconnected protein network of de novo mutations. *Nature* *485*, 246–250.
- Orekhova, E.V., Elsabbagh, M., Jones, E.J., Dawson, G., Charman, T., and Johnson, M.H.; BASIS Team (2014). EEG hyper-connectivity in high-risk infants is associated with later autism. *J. Neurodev. Disord.* *6*, 40.
- Osorio-Gomez, D., Guzman-Ramos, K., and Bermudez-Rattoni, F. (2017). Memory trace reactivation and behavioral response during retrieval are differentially modulated by amygdalar glutamate receptors activity: interaction between amygdala and insular cortex. *Learn. Mem.* *24*, 14–23.
- Palmer, L.M., Schulz, J.M., Murphy, S.C., Ledergerber, D., Murayama, M., and Larkum, M.E. (2012). The cellular basis of GABA(B)-mediated interhemispheric inhibition. *Science* *335*, 989–993.
- Pape, H.C., and Driesang, R.B. (1998). Ionic mechanisms of intrinsic oscillations in neurons of the basolateral amygdaloid complex. *J. Neurophysiol.* *79*, 217–226.
- Paré, D., Pape, H.C., and Dong, J. (1995). Bursting and oscillating neurons of the cat basolateral amygdaloid complex in vivo: electrophysiological properties and morphological features. *J. Neurophysiol.* *74*, 1179–1191.
- Ribolsi, M., Daskalakis, Z.J., Siracusano, A., and Koch, G. (2014). Abnormal asymmetry of brain connectivity in schizophrenia. *Front. Hum. Neurosci.* *8*, 1010.
- Roosendaal, B., McEwen, B.S., and Chattarji, S. (2009). Stress, memory and the amygdala. *Nat. Rev. Neurosci.* *10*, 423–433.
- Rumpel, S., LeDoux, J., Zador, A., and Malinow, R. (2005). Postsynaptic receptor trafficking underlying a form of associative learning. *Science* *308*, 83–88.
- Sanders, S.J., He, X., Willsey, A.J., Ercan-Sencicek, A.G., Samocha, K.E., Cicek, A.E., Murtha, M.T., Bal, V.H., Bishop, S.L., Dong, S., et al.; Autism Sequencing Consortium (2015). Insights into Autism Spectrum Disorder Genomic Architecture and Biology from 71 Risk Loci. *Neuron* *87*, 1215–1233.

- Sosulina, L., Meis, S., Seifert, G., Steinhäuser, C., and Pape, H.C. (2006). Classification of projection neurons and interneurons in the rat lateral amygdala based upon cluster analysis. *Mol. Cell. Neurosci.* *33*, 57–67.
- Stachniak, T.J., Ghosh, A., and Sternson, S.M. (2014). Chemogenetic synaptic silencing of neural circuits localizes a hypothalamus→midbrain pathway for feeding behavior. *Neuron* *82*, 797–808.
- Stujenske, J.M., Likhtik, E., Topiwala, M.A., and Gordon, J.A. (2014). Fear and safety engage competing patterns of theta-gamma coupling in the basolateral amygdala. *Neuron* *83*, 919–933.
- Suárez, R., Gobius, I., and Richards, L.J. (2014). Evolution and development of interhemispheric connections in the vertebrate forebrain. *Front. Hum. Neurosci.* *8*, 497.
- Thurley, K., Leibold, C., Gundlfinger, A., Schmitz, D., and Kempfer, R. (2008). Phase precession through synaptic facilitation. *Neural Comput.* *20*, 1285–1324.
- Tovote, P., Fadok, J.P., and Lüthi, A. (2015). Neuronal circuits for fear and anxiety. *Nat. Rev. Neurosci.* *16*, 317–331.
- Valera, E.M., Faraone, S.V., Murray, K.E., and Seidman, L.J. (2007). Meta-analysis of structural imaging findings in attention-deficit/hyperactivity disorder. *Biol. Psychiatry* *61*, 1361–1369.
- Watabe, A.M., Ochiai, T., Nagase, M., Takahashi, Y., Sato, M., and Kato, F. (2013). Synaptic potentiation in the nociceptive amygdala following fear learning in mice. *Mol. Brain* *6*, 11.
- Wessa, P. (2019). *Free Statistics Software. Office for Research Development and Education, version 1.2.1.* <https://www.wessa.net>.
- Xu, K., Jiang, W., Ren, L., Ouyang, X., Jiang, Y., Wu, F., Kong, L., Womer, F., Liu, Z., Blumberg, H.P., et al. (2013). Impaired interhemispheric connectivity in medication-naïve patients with major depressive disorder. *J. Psychiatry Neurosci.* *38*, 43–48.
- Yizhar, O., Fenno, L.E., Prigge, M., Schneider, F., Davidson, T.J., O’Shea, D.J., Sohal, V.S., Goshen, I., Finkelstein, J., Paz, J.T., et al. (2011). Neocortical excitation/inhibition balance in information processing and social dysfunction. *Nature* *477*, 171–178.

STAR★METHODS

KEY RESOURCES TABLE

REAGENT or RESOURCE	SOURCE	IDENTIFIER
Antibodies		
c-FOS (rabbit)	Cell Signaling	9F6; RRID: AB_2247211
CaMKII α (mouse)	Millipore Chemicon	MAB8699; RRID: AB_2067919
MEF2C (rabbit)	Proteintech	10056-1; RRID: AB_513447
GAD67 (mouse)	Sigma	G5419; RRID: AB_261978
GFP (chicken)	Abcam	ab13970; RRID: AB_300798
DsRed (rabbit)	Clontech	632496; RRID: AB_10013483
Chemicals, Peptides, and Recombinant Proteins		
Neurobiotin™ Tracer	Vector Laboratories	SP-1120
CNQX	Tocris	0190
Tetrodotoxin citrate	Tocris	1069
Clozapine N-oxide	Enzo Life Sciences	BML-NS105-0005
D-cycloserine	Abcam	Ab120121
Ifenprodil	Sigma	12892-25MG
D-APV	Tocris	0106
Retrobeads, red	Lumafuor Inc.	Red Retrobeads™ IX
Retrobeads, green	Lumafuor Inc.	Green Retrobeads™ IX
Experimental Models: Organisms/Strains		
<i>Mus musculus</i> / C57BL/6J	National Animal Research Laboratory, Taiwan	N/A
Recombinant DNA		
AAV-CaMKII α -hChR2(C128S/D156A)-EYFP	Dr. Karl Deisseroth	Addgene plasmid #35501 (Yizhar et al., 2011)
AAV-CaMKII α -hChR2(H134R)-EYFP	Dr. Karl Deisseroth	Lee et al., 2010
AAV-oChIEF-citrine	Dr. John Lin	Lin et al., 2009
AAV-oChIEF-tdTomato	Dr. John Lin	Addgene #50977 (Lin et al., 2009)
AAV-CaMKII α -hM4D(Gi)-mCherry	Dr. Bryan Roth	Addgene #50477-AAV8 (Nawaratne et al., 2008)
Software and Algorithms		
GraphPad Prism	GraphPad Software	Version 5.0 or 7.0
SigmaStat	Systat Software	Version 3.5
Free Statistics Software	Wessa, 2019	Version 1.2.1
Clampfit	Molecular Devices	Version 10.7
Signal	Cambridge Electronic Design	Version 4
FreezeScan	CleverSys Inc.	Version 2.0
Imaris	BitPlane	Version 9.2.1
Zen	Carl Zeiss	Version 10
ImageJ	Nation Institutes of Health	Version 1.50b
DC2100	ThorLABS	Version 1.3
MetaXpress	Molecular Devices	Version 6.2.3.733
Amira	ThermoFisher Scientific	Version 6.4

LEAD CONTACT AND MATERIALS AVAILABILITY

Requests for further information should be directed to and will be fulfilled by the Lead Contact, Yi-Ping Hsueh (yph@gate.sinica.edu.tw). This study did not generate new unique reagents.

EXPERIMENTAL MODEL AND SUBJECT DETAILS

Male C57BL/6J mice at 6–8 weeks of age purchased from the National Animal Research Laboratory, Taiwan, were used for all experiments in this report. The *Tbr1*^{+/-} mice (Bulfone et al., 1998) were originally provided by Drs. R. F. Hevner (Department of Neurological Surgery, University of Washington, Seattle) and J. L. Rubenstein (Department of Psychiatry, University of California, San Francisco). Mice were housed in the animal facility of the Institute of Molecular Biology, Academia Sinica, under controlled temperature and humidity and a 12 h light/12 h dark cycle. All animal experiments were performed at 2–4 months of age with the approval of the Academia Sinica Institutional Animal Care and Utilization Committee and in strict accordance with its guidelines (Protocol No. 14-11-759).

METHOD DETAILS

Production of pseudotyped AAV8 vectors

AAV production was performed as described (Chen et al., 2009; Lin, 2013) or with some modification. Briefly, AAV constructs encoding hChR2-eYFP fusion protein under the control of the calcium calmodulin kinase II (CamKII) promoter and the construct encoding oChIEF with fluorescent protein (Citrine or tdTomato) fusion under the control of the human synapsin promoter were used. Pseudotyped AAV8 vectors were produced by triple-plasmid transfection and purified by two rounds of CsCl centrifugation or iodixanol gradient centrifugation. The physical vector titers were quantified by measuring the number of packaged vector genomes by real-time PCR using SYBR Green reaction mix (Roche Diagnostics, Mannheim, Germany).

Stereotaxic surgery, probe implantation and injection of AAV and retrograde microbeads

Mice were deeply anesthetized and placed on a Lab Standard Stereotaxic Instrument (Stoelting, Wood Dale, IL USA). After securing the animal to restrict its movement, 0.3 μ L AAV solution (10^{10} vg/ μ L) with or without Red RetrobeadsTM IX (Lumafuor Inc.) was slowly infused over 10 min into the basolateral amygdala (BLA) (1.70 mm posterior, 3.3 mm lateral and 4.5 mm ventral to the bregma). To monitor the retrograde signal from the central amygdala (CeA) to the BLA, 0.1 μ L Green RetrobeadsTM IX (Lumafuor Inc.) were infused into the CeA (1.58 mm posterior, 2.8 mm lateral and 4.3 mm ventral to the bregma). After a two- to three-week recovery, expression of channelrhodopsin-fluorescent proteins at the axonal termini of BLA neurons was confirmed by fluorescence or confocal laser scanning microscope during or after electrophysiological recording or behavioral analyses. Sites of probe implantation, AAV injection and pharmaceutical treatment at BLA were indicated in Figure S8

Optogenetic stimulation for C-FOS staining

Two weeks after AAV8 injection, mice were anesthetized by 2.5% isoflurane and stimulated with a 470 nm LED light (0.5 mW/mm² at the tip of optical fiber) at 10 ms, 20 Hz for 20 s four times with 1-min intervals. Two hours after stimulation, mice were sacrificed for immunofluorescence staining (see below).

Chemogenetic study

Mice were infused with 0.3 μ L of AAV (either AAV8-CaMKIIa-hM4D(Gi)-mCherry ($\geq 2 \times 10^{12}$ vg/ml) or AAV8-CamKII-hChR2(128S/D156A)-eYFP (10^{13} vg/ml)) into one side of the BLA. Guide cannulas (Plastics One) were implanted at the other side of the BLA. Two weeks later, mice were ready for behavior tests (see “Behavioral analyses” below). Thirty minutes before tasks, 0.1 μ L CNO (0.1 μ g/ml) was locally injected through the guide cannula at a speed of 50 nL/min.

Slice electrophysiology

Mice were anesthetized with isoflurane and transcardially perfused with ice-cold carbogenated (95% O₂ and 5% CO₂) sucrose solution (~30 mL) containing (in mM): 87 NaCl, 25 NaHCO₃, 1.25 NaH₂PO₄, 2.5 KCl, 10 glucose, 75 sucrose, 0.5 CaCl₂, and 7 MgCl₂. Brains were dissected and sectioned in the same carbogenated sucrose solution using a vibrating tissue slicer (MicroslicerTM DTK-1000, Dosaka). Coronal slices (300 μ m thick) were prepared from AAV8-injected mice at least 3 weeks after surgery. After incubating the slices at 34°C for 25 min and allowing recovery at room temperature (23 \pm 2°C) in a holding chamber for at least 90 min, individual slices were then transferred to a submerged chamber for recording. The submerged chamber was continuously perfused with carbogenated artificial cerebrospinal fluid (ACSF) containing the following (in mM): 125 NaCl, 25 NaHCO₃, 1.25 NaH₂PO₄, 2.5 KCl, 25 glucose, 2 CaCl₂, and 1 MgCl₂. Expression of AAV8 at axonal termini was confirmed by fluorescence microscope. Neurons were visually selected for recordings under an infrared differential interference contrast (IR-DIC) microscope (SliceScope, Scientifica) connected to a CCD camera (IR-1000, DAGE-MTI). Whole-cell recordings were performed with patch pipettes (4–8 M Ω) filled with the internal solution consisting of the following (in mM): 135.25 K-gluconate, 8.75 KCl, 0.2 EGTA, 4 MgATP, 10 HEPES, 7 Na₂-phosphocreatine, 0.5 Na₃GTP (pH 7.3 with KOH), and 0.3% neurobiotin (wt/vol; Vector Laboratories). Cs-based intracellular solution was used to measure the inhibitory (I)–excitatory (E) conductance ratio, which consisted of (in mM): 121.5 CsMeSO₃, 0.1 EGTA, 4 MgATP, 13.5 CsCl₂, 10 HEPES, 5 QX-314 bromide, 7 Na₂-phosphocreatine, 0.3 Na₃GTP, and 0.3% neurobiotin (wt/vol). For optogenetics, synaptic responses were evoked by light-pulse stimulation (6.6 mW/mm², 5 or 10 ms duration, 20 s inter-sweep interval) of axonal termini expressing ChR2 in the contralateral BLA with a 470 nm light (OptoLED Light Source, Cairn Research Ltd) delivered through a

40x NA/0.8 water immersion objective (LUMPLFLN; Olympus). The optical stimuli were simultaneously recorded by a GaP photodiode (wavelength range: 150–550 nm, 1 ns rise time, Thorlabs). For electrical stimulation of cortical inputs or thalamic inputs, the external capsule or internal capsule was stimulated (200 μ s) with a monopolar electrode, respectively. We compensated for pipette capacitance and series resistance (R_s) (70% in voltage-clamp and 100% in current-clamp). For pharmacological experiments, R_s or input resistance (R_{in}) were monitored in each sweep. Data were discarded if R_s or R_{in} changed by >20% during the recording period. Data were recorded with Multiclamp 700B amplifiers (Molecular Devices), filtered at 3 kHz, and sampled at 10 kHz with a Power 1401 mk II digitizer (Cambridge Electronic Design) controlled by Signal 4 software (Cambridge Electronic Design). The recording temperature was $23 \pm 2^\circ\text{C}$. Data were analyzed offline using Clampfit 10.7 (Molecular Devices). Postsynaptic current (PSC) and postsynaptic potential (PSP) amplitude (calculated from the pre-stimulation membrane potential to the peak of the PSP evoked by electrical or optical stimulation) were analyzed for pharmacological experiments, I:E ratio calculation, multiple-pulse ratio measurement (EPSC_n amplitude divided by EPSC_1 amplitude) and the potentiation effect of contralateral BLA afferents. To distinguish projection neurons (PNs) from interneurons (INs), three intrinsic action potential properties were recorded: (1) maximal mean firing rate measured the maximal number of spikes in response to prolonged current injection within 1 s; (2) spike firing adaption was calculated from the firing trains at the maximal mean firing rate and was expressed as the ratio of instantaneous firing frequency difference between the first two spikes (f_{initial}) and 200 ms after current injection (f_{200}) to the f_{initial} ; (3) fast afterhyperpolarization amplitude was measured from the first spike evoked by threshold current injection, which is defined as the amplitude from the baseline (plateau potential without a spike during the current injection period) to the first negative peak of the hyperpolarization phase following the spike peak. To further confirm that these three action potential properties were suitable for classifying PNs and INs, hierarchical clustering using squared Euclidean distances and Ward's method was conducted. Variables of three action potential properties in each neuron were first transformed into the range (0, 1) by min-max normalization, and hierarchical clustering was performed using Free Statistics Software v.1.2.1 (Wessa, 2019).

Immunofluorescence staining

After perfusion with 4% paraformaldehyde in PBS, the brains were dissected and postfixed with 4% paraformaldehyde overnight at 4°C . Brains were cryopreserved in 30% sucrose at 4°C for two days and embedded in OCT (4583, Tissue-Tek). Fifty- μm -thick brain sections were cut with a cryostat microtome (CM1900, Leica). After rinsing with PBS, permeabilization was performed with 0.3% Triton X-100 in PBS (PBST) and blocked with 3% horse serum and 2% bovine serum albumin (BSA) in PBST at room temperature for 2 h. Primary antibodies (anti-C-FOS (1:200), anti-GFP (1:5000), anti-CaMKII (1:500), anti-MEF2C (0.93 $\mu\text{g}/\text{ml}$), or anti-GAD67 (1:250)) were then added for overnight incubation at 4°C . After washing, sections were incubated with Alexa fluor 488- and/or 555-conjugated secondary antibodies (Invitrogen, Inc.). The numbers of C-FOS-positive cells were then measured with ImageJ (NIH). For neurobiotin and fluorescent protein double staining after electrophysiological recording, brain slices were postfixed and the staining protocol was conducted as described above. Anti-GFP (1:5000) or anti-DsRed antibodies combined with Alexa fluor 488 or Alexa fluor 555-conjugated secondary antibody was used to visualize fluorescent protein signals. Neurobiotin signals were revealed by streptavidin-conjugated Alexa Fluor 647 or streptavidin-conjugated Alexa Fluor 488 (1:400; Invitrogen, Inc.). To analyze whether different retrobead and C-FOS immunoreactivities co-existed in BLA neurons, each channel of image files was set a threshold of intensity in ImageJ (NIH). Image remerging, marker labeling and atlas replacement were processed using Photoshop (Adobe). The stepwise procedure for this analysis is described in [Figure S7](#).

Confocal microscopy, imaging, and Imaris 3D construction

Confocal images were acquired at room temperature using an LSM700 microscope (Carl Zeiss) equipped with a $20 \times$ NA 0.8 or $63 \times$ /NA 1.4 oil objective lens (Plan-Apochromat; Carl Zeiss) and Zen 2009 acquisition and analysis software (Carl Zeiss). For 3D reconstruction, Z stack images of BLA neurons were generated with the Imaris software (BitPlane, MN, USA). The 3D videos are available online in Supplemental Materials. For publication, images were exported and processed using Photoshop (Adobe) with minimal adjustments to the brightness and/or contrast of entire images.

Behavioral analyses

Two to three-month-old male mice were randomly chosen for surgery and transferred to a behavioral room and single-housed for at least 14 days. Behavioral assays were carried out from 11:00~18:00, at least two hours before the dark cycle. Mice were randomly selected for reciprocal social interaction (RSI), followed by conditional taste aversion (CTA) tests. Intervals between paradigms were about 7 days. Behavioral analyses were performed blind.

RSI-

RSI was performed as described ([Huang et al., 2014](#)). Briefly, test mice were individually housed for at least 7 days. During the test session, an unfamiliar mouse was put into the home cage of the isolated test mouse without replacing the lid of the cage. The social interaction of the test mouse with the unfamiliar mouse was recorded for 3 min using a digital camera. The time that the test mouse spent interacting with the unfamiliar mouse was measured to indicate RSI.

CTA-

The procedures for the CTA behavioral test were described previously ([Chung et al., 2011](#)). Briefly, after pretraining for 7 days, mice were presented with a sucrose-lithium chloride (LiCl) pairing, whereby they were first offered a sucrose solution (pleasant, new taste;

100 mM, 15 min) followed by an intraperitoneal injection of LiCl (malaise-inducing agent; 0.15 M, 20 μ l/g of body weight). Diarrhetic response in mouse home cages was observed. As a control, NaCl instead of LiCl was injected into mice so that control animals did not experience malaise. Volumes of water drank on the last pretraining day and of sucrose solution on the training day were recorded to ensure normal water and sucrose uptake. Two days after training, mice were presented with two bottles (one water, one 100 mM sucrose) for 15 min. Amounts of sucrose and water drank were recorded to measure the sucrose preference index = sucrose intake / (sucrose + water intake). A reduced sucrose preference in the two-bottle test indicated memory of the CTA.

Pharmacological treatment

For local infusion, one 25-gauge stainless steel guide tube was implanted into the amygdala (1.7 mm posterior, 3.1 mm lateral and 4.7 mm ventral to the bregma). A 30-gauge dummy cannula was put into the guide tube to prevent clogging. Two screws were fixed to the skull and dental cement was used to fasten the guide tube onto the skull. After recovery for two weeks, ifenprodil (2 mg/ml, Sigma) or normal saline was unilaterally injected into amygdalae at a rate of 0.5 μ l/min. Thirty minutes after administration with ifenprodil, mice were ready for behavior tests.

QUANTIFICATION AND STATISTICAL ANALYSIS

Data are presented as means plus SEM, except [Figure S4D](#) (means plus s.d.). Data from individual animals are indicated as dots in the figures. Animals were randomly chosen for experiments. Behavioral assays were conducted blind. No statistical method was applied to evaluate the sample size, but our sample sizes are similar to previous publications ([Huang et al., 2014](#); [Huang and Hsueh, 2017](#)). Data meet the assumption of the tests, e.g., normal distribution. Statistical comparisons were performed with two-way repeated-measures ANOVA with post hoc Bonferroni's test, unpaired or paired Student's t tests, and Wilcoxon matched-pairs signed rank test using SigmaStat 3.5 (Systat Software) or GraphPad Prism 5.0 (5.0 or 7.0, GraphPad Software) as indicated in the figure legends.

DATA AND CODE AVAILABILITY

There is no dataset/code associated with the paper.